

# Lattice-driven femtosecond magnon dynamics in $\alpha$ -MnTe

Kira Deltenre,<sup>1</sup> Davide Bossini,<sup>2</sup> Frithjof B. Anders,<sup>1</sup> and Götz S. Uhrig<sup>1</sup>

<sup>1</sup>*Condensed Matter Theory, Department of Physics,  
TU Dortmund University, 44227 Dortmund, Germany*

<sup>2</sup>*Department of Physics and Center for Applied Photonics,  
University of Konstanz, D-78457 Konstanz, Germany*

(Dated: December 13, 2021)

The light-induced femtosecond dynamics of the sublattice magnetizations in the antiferromagnetically ordered phase of the semiconductor  $\alpha$ -MnTe is investigated theoretically as function of an external driving field. The electromagnetic field is coupled to optical modes and the concomitant atomic displacements modulate the Heisenberg exchange couplings. We derive the equations of motion for the time-dependent sublattice magnetization in spin wave theory and analyze the contributions from the driven magnon modes. The antiferromagnetic order parameter exhibits coherent longitudinal oscillations determined by the external driving frequency which decay due to dephasing. Including a phenomenological dissipative term to mimic spin-lattice relaxation processes leads to relaxation back to thermal equilibrium. We provide approximate analytic solutions of the resulting differential equations which allow us to understand the effect of the driving light pulse on the amplitude, frequency, and lifetime of the coherent spin dynamics.

## I. INTRODUCTION

The interaction between light and matter is one of the central current issues of condensed matter physics due to the various types of magnetic and electronic order and different essential interactions in materials. Besides the general understanding of light-matter interactions, specifically, controlling the magnetic order of solids with light [1–6] could be the required milestone to develop spintronic devices working on unprecedented timescales. In experiments, femtosecond laser pulses have already realised the ultrafast all-optical switching of the magnetisation in a wide variety of materials [1, 3], femtosecond magnetic phase transitions [7–9], and the coherent generation of magnons [2, 10–12], even with the mediation of the lattice [13]. The latter effect is particularly relevant for more reasons: (i) coherent mechanisms provide the possibility to manipulate spins without energy dissipation; (ii) the magnetoelastic coupling is almost ubiquitous and significantly strong in antiferromagnets [14, 15] which are highly promising and heavily investigated compounds.

Here, we focus on a specific strongly correlated compound, namely hexagonal manganese telluride ( $\alpha$ -MnTe) [16]. It is a magnetic semiconductor with indirect bandgap in the near infrared range ( $E_g = (1.27–1.46)$  eV [17]). While the semiconducting properties arise from the Te  $5p$  orbitals and the Mn  $4s$  orbitals, the material exhibits an antiferromagnetic (AF) order of the Mn  $3d$  spins consisting of ferromagnetically ordered layers of spins which are antiparallel between adjacent layers below the Néel temperature  $T_N \approx 310$  K [17]. It is found that the electronic band gap is influenced by the degree of magnetic order. In fact, an additional contribution to the band gap proportional to the square of the sublattice magnetization occurs [18, 19].

This material has been experimentally proven to possess a substantial spin-lattice coupling, since both the frequency and the lifetime of two degenerate Raman-

active phonon modes with 5.3 THz frequency are significantly affected by the establishment of the long-range magnetic order [20]. Hexagonal MnTe is thus a representative choice for the material class of dielectric correlated antiferromagnets. The correlated nature is in fact common to a massive variety of other compounds (e.g. oxides) and the strong magneto-acoustic coupling is almost ubiquitous in antiferromagnets [15, 20]. So far two phonon-magnon coupling mechanisms have been considered to interpret observations on the femtosecond time-scale: the nonlinear phononics [13, 21] and the Kittel mode [22].

A very recent time-resolved experiment [23] displays photo-induced coherent oscillations of the rotation of the polarisation of light well pronounced in the antiferromagnetic phase of  $\alpha$ -MnTe. In this experiment, femtosecond laser pulses trigger the 5.3 THz modes by means of a Raman-scattering mechanism changing the interatomic potentials for fractions of a picosecond. This displacive effect constitutes the pumping mechanism. Moreover, the dispersion of magnons of the material [24] excludes the physical framework of the Kittel mode because magnons and phonons do not display an avoided crossing in their dispersions. A novel physical mechanism has thus to be explored to interpret the observations, which are expected not to be limited to  $\alpha$ -MnTe, given the generality of the formulation.

The question arises how light couples to the magnetic subsystem and coherently drives a magnetization modulation in the class of antiferromagnetically ordered insulators (or semiconductors) [23]. Based on the seminal work by Fleury and Loudon [25] and Shastry and Shraiman [26] it is possible that Raman scattering directly excites spin degrees of freedom via the Peierls coupling of the vector potential in the hopping elements of the underlying fermionic Hubbard model. This mechanism has been recently invoked to compute the magnon circular photogalvanic effect [27]. The mapping of the fermionic model on the spin model works best if the Raman pumping is

performed off resonance. But in this regime the excitation of magnetic dynamics tends to be rather inefficient.

In contrast to the direct coupling of light to the spins via a Peierls substitution in the underlying Hubbard model [26], the aforementioned dominant coupling of optical phonons to the spin degrees of freedom, is revealed by Raman spectroscopy [20]. This coupling can be qualitatively understood since the superexchange paths pertinent to the magnetic couplings depend on the overlaps of the atomic orbitals, which are determined by the ionic positions and possible motions thereof. This is a key ingredient for creating magnetic excitations.

Such atomic motion can be triggered by so called displacive stimulated Raman scattering. The excitation of an electron from an occupied to an unoccupied state alters the interionic potentials so that the previous atomic positions are no longer equilibrium positions. Hence the atoms start moving towards the minima of the modified potential. This induces a coherent oscillatory motion of the atomic positions in each unit cell that is governed by the optical phonon frequencies. This oscillatory motion persists once the electronic excitations has decayed on the short time scale of hundreds of femtoseconds. This periodic modulation of the Mn-Te distances and angles in the unit cell translates into a periodic modulation of the tight-binding hopping parameters of an effective Hubbard model for the manganese  $3d$  subsystem. According to the relation  $J \propto t^2/U$  between the magnetic exchange  $J$ , the hopping  $t$  and the on-site repulsion  $U$  the periodic modulation of  $t$  entails a periodic modulation of the exchange coupling [28].

This leads us to a coupling mechanism by means of displacement based on the modulation of the Heisenberg exchange couplings in an effective spin model for the magnetic degrees of freedom. This optomagnetic mechanism is similar to the one recently studied for a disordered spin system [29]. The key difference is the way how the phonons or atomic displacements are pumped by light. Infrared active phonons can be set into motion directly by THz radiation while we invoke displacive stimulated Raman scattering in the present work.

A indirect magneto-phononic coupling was considered in the context of  $\text{Cr}_2\text{O}_3$ . The assumption was made in Ref. [28] that an infrared vibrational model is driven by sinusoidal laser field in the THz range, and is coupled via non-linear terms to an effective Heisenberg model by a Raman mode. The magnetization dynamics was calculated by a phenomenological Landau-Lifshitz-Gilbert equation.

In the present paper, we are guided by the experimental setup [23] where a very short fs laser pulse with spectral range centred at 1.71 eV slightly above the band gap induces atomic displacements on an ultrashort time scale leading to a coherent optical lattice mode which drives the magnetic subsystem on a ps time scale. The amplitude of the lattice mode decays exponentially on the ps time scale due to coupling to the bath of acoustic phonons. In particular, we are interested in the quantum mechanical description of the change in the sublattice

magnetization of the antiferromagnet as function of time.

Starting from the modulated Heisenberg exchange couplings [28], we employ Holstein-Primakoff linear spin-wave theory out of equilibrium to calculate the generation of magnon pairs and the induced dynamics of the sublattice magnetization for various system parameters such as the driving frequency, the driving intensity, and the pulse duration. We also include spin-lattice relaxation on the level of a Markov approximation to describe the realistic long-time relaxation of the optically activated system.

Our approach is generic for lattice-driven magnon dynamics in ordered quantum magnets leading to a universal analytic structure of the equations of motion. The material specific details only enter in the modifications of momentum dependent couplings in the differential equations, but they do not change their analytic structure. Using realistic exchange couplings extracted from measured magnon dispersions [30] allows us to make contact to the lattice-driven femtosecond magnon dynamics in  $\alpha$ -MnTe [23].

This article is structured as follows. We present the underlying Heisenberg spin model in Sec. II A and its treatment by Holstein spin-wave theory in Sec. II B where we establish the equilibrium properties in the antiferromagnetic symmetry broken phase. Section III is devoted to the non-equilibrium dynamics. We derive the generic equation of motion for the driven magnon dynamics in Sec. III A and discuss the properties in Sec. III B where we present approximate analytic solutions of the equations. The accuracy of the approximations is demonstrated by a comparison with the numerical solution of the full dynamics. Section III C is devoted to the various aspects of the dynamics of the sublattice magnetization as induced by the pulses. We use the developed theoretical framework to make contact to the magnon dynamics in  $\alpha$ -MnTe in Sec. IV. The paper is finished with conclusion and outlook in Sec. V.

## II. THEORY

The focus of our work are the collective magnetic excitations of an antiferromagnet and, in particular, their coupling to the lattice. Therefore, we focus on the purely magnetic description based on an effective Heisenberg model.

### A. Model

The unit cell of hexagonal MnTe with NiAs structure consists of two Mn-ions and two Te-ions as depicted in Fig. 1. At each Mn-site, a magnetic moment of  $S = 5/2$  is localized. The Mn-sites are arranged in layers of stacked triangular lattices. The spins within each triangular layer are aligned in a parallel way. The spins of the adjacent layers are antiparallel to each other as indicated by the arrows in Fig. 1. The two Mn-ions in the unit cell belong to

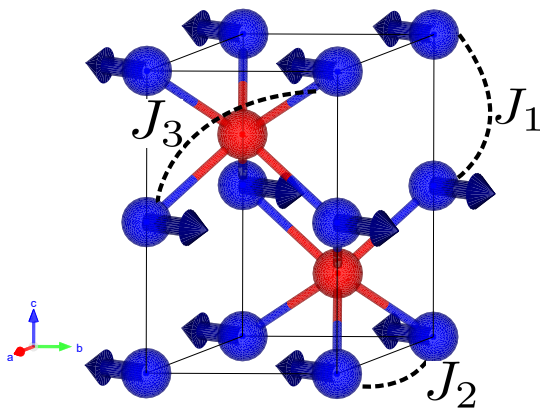


FIG. 1. The unit cell of  $\alpha$ -MnTe consists of two Mn-ions (blue) and two Te-ions (red). On the Mn-sites, magnetic moments are localized. Image made with VESTA [31].

different sublattices which are defined by the orientation of the spins. The model captures the magnetic moments localized at the Mn-sites. The orbitals of the Te-ions allow for virtual hopping processes generating exchange couplings. They do not need to be considered explicitly here.

The hybridization between the Mn-Mn and Mn-Te orbitals mediate effective Heisenberg couplings between the localized  $S = 5/2$  Mn  $3d$  moments. The resulting low-temperature spin Hamiltonian reads

$$H = J_1 \sum_{\langle i,j \rangle_c} \vec{S}_i \vec{S}_j + J_2 \sum_{\langle i,j \rangle_{ab}} \vec{S}_i \vec{S}_j + J_3 \sum_{\langle\langle i,j \rangle\rangle} \vec{S}_i \vec{S}_j \quad (1)$$

as derived in Refs. [24, 30]. The model includes three terms: an antiferromagnetic interlayer coupling  $J_1 > 0$  between nearest neighbors (NN) along the  $c$ -axis, a ferromagnetic in-plane coupling  $J_2 < 0$ , and an antiferromagnetic third-nearest-neighbor coupling  $J_3 > 0$ . In Ref. [30] the values for the parameters were obtained by a fit to inelastic neutron scattering data based on spin-wave theory leading to the values  $J_1 = 21.5$  K,  $J_2 = -0.67$  K, and  $J_3 = 2.87$  K. Due to the different notation of the Hamiltonian, the signs are different in this work, and a factor 2 is included.

The interaction between femtosecond laser pulses and MnTe is expected to induce coherently Raman active phonons, either via the impulsive stimulated Raman scattering [32] or displacive excitation of coherent phonons mechanism [33]. In particular, the 5.3 THz modes aforementioned are optical phonons and they modify the exchange coupling, as they correspond to Te-atoms oscillations [23]. We consider the resonant excitation of a particular phonon at frequency  $\omega_0$ . Hence, this is also the frequency by which the the exchange couplings are modulated. We assume that the parameter  $J_3$ , which couples third-nearest-neighbor spins via a Te-ion, changes its value due to the relative oscillation of the Mn- and the Te-ions. We include this effect in the Hamiltonian by a time-dependent coupling

$$J_3 \rightarrow J_3(t) = J_3^{(0)} + \delta J_3(t) \quad (2)$$

where  $J_3^{(0)}$  is the equilibrium exchange coupling and  $\delta J_3(t)$  parametrizes the effect of the laser field via the phonon on the magnetic subsystem. In general, the other exchange parameters can also change in time. But for clarity, we stick to the modulation of  $J_3$  for the majority of calculations. The modulation of the other couplings is considered in Sec. IV B and it turns out that the effect of modulated  $J_1$  or  $J_2$  is qualitatively very similar and does not lead to qualitatively different phenomena.

## B. Method

In order to analyze the non-equilibrium dynamics of the order parameter, we first determine the equilibrium model by resorting to a linear spin waves ansatz [34, 35] for the AF phase. As a first step, we invert all spins of one sublattice such that the mapped problem has ferromagnetic spin order. In a second step, we employ the Holstein-Primakoff representation [36] which represents the spin operators by bosonic operators

$$S_i^z = -S + \tilde{b}_i^\dagger \tilde{b}_i \quad (3a)$$

$$S_i^+ = \tilde{b}_i^\dagger \sqrt{2S - \tilde{b}_i^\dagger \tilde{b}_i} \approx \sqrt{2S} \tilde{b}_i^\dagger \quad (3b)$$

$$S_i^- = \sqrt{2S - \tilde{b}_i^\dagger \tilde{b}_i} \tilde{b}_i \approx \sqrt{2S} \tilde{b}_i \quad (3c)$$

keeping only the leading order in a  $1/S$  expansion. This is an excellent approximation in the AFM phase because of the large spin  $S = 5/2$  and the large number of coupled neighboring spins. The  $z$ -direction in spin space is defined by the orientation of the spins of sublattice A in the ordered phase. Note that  $z$ -axis of the spin lies in fact in the  $ab$ -plane in real space and that we choose  $\tilde{b}$  for the bosonic operators at the lattice sites and will use  $b$  later in the diagonal Bogoliubov representation.

Note that we only have to deal with bilinear terms in leading order. Thereby, interactions between different  $\vec{k}$ -modes are neglected; in this approximation they do not scatter from each other. In addition, relaxation mechanisms are not included in our model so far. The Fourier transform

$$\tilde{b}_i = \frac{1}{\sqrt{N}} \sum_{\vec{k}} \exp(i\vec{k} \cdot \vec{l}) \tilde{b}_{\vec{k}}, \quad (4)$$

into momentum space yields the dimensionless Hamiltonian

$$\frac{H_0}{J_1 S} = E_d + \sum_{\vec{k}} \left[ A_{\vec{k}} \tilde{b}_{\vec{k}}^\dagger \tilde{b}_{\vec{k}} + \frac{1}{2} B_{\vec{k}} \left( \tilde{b}_{\vec{k}}^\dagger \tilde{b}_{-\vec{k}}^\dagger + \text{h.c.} \right) \right] \quad (5)$$

where we use the coefficients

$$A_{\vec{k}} := \frac{1}{J_1} \left( 2J_1 - 6J_2 + 12J_3 + J_2 \gamma_\Delta(\vec{k}) \right) \quad (6a)$$

$$B_{\vec{k}} := 2 \cos(k_c) \left( 1 + 2 \frac{J_3}{J_1} \gamma_\Delta(\vec{k}) \right) \quad (6b)$$

$$\gamma_\Delta(\vec{k}) := \cos(k_a) + \cos\left(\sqrt{3}k_b/2 + k_a/2\right) + \cos\left(-\sqrt{3}k_b/2 + k_a/2\right). \quad (6c)$$

The Hamiltonian is diagonal in  $k$ -space except for the coupling of  $\vec{k}$  and  $-\vec{k}$  in the creation and annihilation terms of pairs of magnons. This also determines how non-equilibrium perturbations in the couplings enter the real-time dynamics investigated below.

The Holstein-Primakoff transformation generates the offset  $E_d$  independent of momentum

$$E_d = -NS \left( 1 - 3\frac{J_2}{J_1} + 6\frac{J_3}{J_1} \right). \quad (7)$$

The Bogoliubov transform

$$\tilde{b}_{\vec{k}} = b_{\vec{k}} \cosh \theta_{\vec{k}} + b_{-\vec{k}}^\dagger \sinh \theta_{\vec{k}} \quad (8)$$

fully diagonalizes the Hamiltonian (5)

$$\frac{H_0}{J_1 S} = \sum_{\vec{k}} \omega_{\vec{k}} b_{\vec{k}}^\dagger b_{\vec{k}} + E_d + \Delta E \quad (9)$$

if the condition for the Bogoliubov angle  $\theta_{\vec{k}}$

$$\frac{B_{\vec{k}}}{A_{\vec{k}}} = -\tanh(\theta_{\vec{k}}) \quad (10)$$

is met. The additional contribution  $\Delta E$  to the ground energy is given by

$$\Delta E = \frac{1}{2N} \sum_{\vec{k}} (\omega_{\vec{k}} - A_{\vec{k}}). \quad (11)$$

It does not influence the magnetic excitations. Finally, we obtain the magnon dispersion in units of  $J_1$

$$\omega_{\vec{k}} = \sqrt{A_{\vec{k}}^2 - B_{\vec{k}}^2}, \quad (12)$$

which is easily evaluated for any given set of couplings  $J_i$ .

### 1. Equilibrium properties

The parameter set stated below Eq. (1) yields the magnon dispersion shown as blue continuous curve in Fig. 2(a) in various directions in the Brillouin zone. We use it for the following calculations. For comparison, the experimental data from Ref. [30] are included as well as black filled circles.

In the calculation of the magnon density-of-states (DOS)

$$\rho(\omega) = \frac{1}{N} \sum_{\vec{k}} \delta(\omega - \omega_{\vec{k}}). \quad (13)$$

for the stacked triangular layers, we profit from the analytical results for triangular lattices in Ref. [37]. The additional vertical component contributes only the term  $\cos(k_c)$  in Eq. (6b). The resulting magnon DOS shown in Fig. 2(b) sets in quadratically

$$f(\omega) = c\omega^2 \quad (14)$$

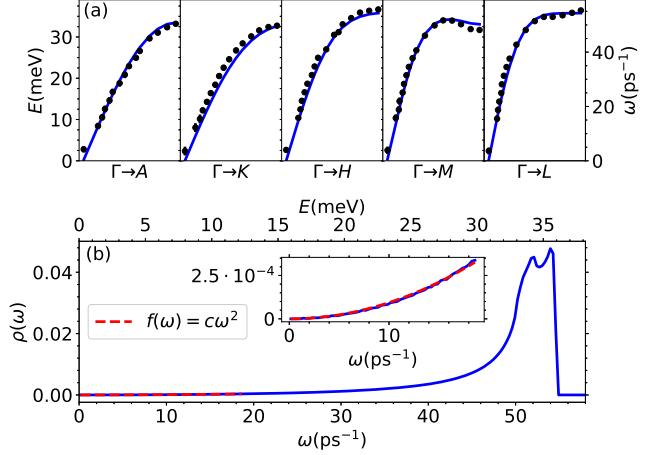


FIG. 2. The magnon dispersion (a) and the magnon density-of-states (DOS) (b). (a) The magnon dispersion measured by inelastic neutron scattering (black dots from Ref. [30]) can be described well by the parameter set proposed in that reference. (b) The corresponding magnon DOS with the parabolic onset (detailed illustration in inset) established for a linear dispersion at low energies in three dimensions. The van Hove singularities appear close to the maximum energy  $\hbar\omega_{\max}$ , i.e., most energies lie close to the  $\hbar\omega_{\max}$ .

with  $c = 9.40(4) \times 10^{-7}$  ps (red dashed line) as implied by the linear dispersion and the three dimensions. The maximum energy  $\hbar\omega_{\max} \approx 35.9$  meV is given by the maximum of the magnon dispersion. In the density of states, we see two peaks that are related to van Hove singularities. The second van Hove singularity is almost at the maximum frequency. Essentially, most frequencies lie close to the maximum frequency.

The order parameter of the antiferromagnetic phase is given by the sublattice magnetization per spin defined as

$$L = \frac{1}{N} \sum_i (-1)^{\delta_i} \langle \hat{S}_i^z \rangle \quad (15)$$

$$\delta_i = \begin{cases} 0 & \text{for sublattice A} \\ 1 & \text{for sublattice B.} \end{cases}$$

We express the order parameter in the framework of spin-wave theory by applying the same transformations as outlined above leading to  $L = L_0 - \delta L$ . The first term  $L_0$  is temperature independent and determined by the spin size  $S = 5/2$  and the quantum fluctuations

$$L_0 = S - \Delta S \quad (16a)$$

$$\Delta S = \frac{1}{2N} \sum_{\vec{k}} \left( \frac{\omega_{\vec{k}}}{A_{\vec{k}}} - 1 \right). \quad (16b)$$

The temperature dependence enters in the second term

$$\delta L = \frac{1}{N} \sum_{\vec{k}} \left[ \frac{A_{\vec{k}}}{\omega_{\vec{k}}} \langle n_{\vec{k}} \rangle - \frac{B_{\vec{k}}}{\omega_{\vec{k}}} \Re \langle b_{\vec{k}}^\dagger b_{-\vec{k}}^\dagger \rangle \right] \quad (17)$$

The second term in the square bracket of Eq. (17) allows us to treat also non-equilibrium situations.

In the case of a driving term in the Hamiltonian,  $\delta L$  becomes time dependent. Due to the upper bound of  $L = 5/2$ , the model only yields reliable results if  $|\delta L| \ll L$ . Thus, the change of the sublattice magnetization  $\delta L$  has to stay significantly smaller than the constant part  $L_0$  in order for the spin wave theory to be applicable. In this paper, we focus on the effect of driving on the sublattice magnetization deep in the ordered phase. We do not consider the effects of finite temperature so that we assume  $T = 0$ .

### III. DYNAMICS OUT OF EQUILIBRIUM

#### A. Magnon dynamics driven by pulses

To describe the dynamics out of equilibrium, we consider the following Hamiltonian [28] including driving

$$H(t) = H_0 + X(t) \quad (18)$$

which consists of the Hamiltonian  $H_0$  of the system in equilibrium and of the time dependent driving  $X(t)$ . The Hamiltonian  $H_0$  and  $H(t)$  are both given by the original form of Hamiltonian, Eq. (1), and only differ in the parameters  $J_i$ . While  $H_0$  only contains the equilibrium values  $J_i^{(0)}$ , the Heisenberg couplings in  $H(t)$  are supplemented by a time-dependent part,  $J_i(t) = J_i^{(0)} + \delta J_i(t)$ .

We include the effect of the laser pulse on the magnetic subsystem of MnTe by time dependent oscillations  $\delta J_3(t)$ . As already mentioned, the laser pulses excite an optical phonon which in turn modifies the exchange path and thereby the exchange coupling [29]. Therefore, we replace  $J_3 \rightarrow J_3^{(0)} + \delta J_3(t)$  in the last term in Eq. (1) and use the resulting term proportional to  $\delta J_3(t)$  as driving operator  $X(t)$ .

After the Bogoliubov transformation it takes the form

$$X(t) = S\delta J_3(t) \sum_{\vec{k}} \left[ \alpha_{\vec{k}} b_{\vec{k}}^\dagger b_{\vec{k}} + \frac{1}{2} \beta_{\vec{k}} \left( b_{\vec{k}}^\dagger b_{\vec{k}}^\dagger + \text{h.c.} \right) + C_{\vec{k}} \right] \quad (19)$$

with the  $\vec{k}$ -dependent coefficients

$$\alpha_{\vec{k}} = \frac{A_{\vec{k}}}{\omega_{\vec{k}}} \left( 12 - 4 \frac{B_{\vec{k}}}{A_{\vec{k}}} \cos(k_c) \gamma_{\Delta}(\vec{k}) \right) \quad (20a)$$

$$\beta_{\vec{k}} = \frac{A_{\vec{k}}}{\omega_{\vec{k}}} \left( -12 \frac{B_{\vec{k}}}{A_{\vec{k}}} + 4 \cos(k_c) \gamma_{\Delta}(\vec{k}) \right). \quad (20b)$$

Note that only equilibrium parameters  $J_i^{(0)}$  enter the Bogoliubov coefficients.

The driving in Eq. (19) includes the crucial term proportional to  $\beta_{\vec{k}}$  creating two magnons. This term is not only the source for incrementing the magnon occupation and other amplitudes, but its also the reason for a frequency doubling in the resonance condition which will be derived below.

Perturbing only the coupling  $J_3$  as a consequence of the excitation of the phonon is one choice among others. We motivate it by the fact that its exchange path runs through the Te-ions so that it is mostly affected by the relative motion of Mn- and Te-ions generated by the lattice dynamics. Nevertheless, we cannot exclude a priori lattice-driven modulations of the other exchange couplings  $J_1$  or  $J_2$ . Their influence is subject of Sec. IV B below. It turns out that only the parameters  $\alpha_{\vec{k}}$  and  $\beta_{\vec{k}}$  need to be changed to account for the modulation of either  $J_1$  or  $J_2$ . But the analytic structure of the differential equations remains unaltered since all interactions are described by a Heisenberg Hamiltonian. The key differences are the coupling strengths  $J_i$  entering in the relative modulation amplitude  $a_0$  introduced below in Eq. (21)) and the number and positions of nearest neighbors spins defining  $\alpha_{\vec{k}}$  and  $\beta_{\vec{k}}$ .

The coefficient  $C_{\vec{k}}$  in Eq. (19) only changes the ground state energy and does not create or annihilate any magnons. For this reason, it is omitted in the following. The remaining part of the operator  $X(t)$  is non-diagonal in the Bogoliubov bosons and drives magnon excitations, i.e., creates or generates them or changes their energy.

The premiss of our work is that an ultrashort laser fs pulse with spectral range centered at 1.71 eV provides a displacement of the charged Mn and Te ions that happens on a fs time scale. The induced damped coherent lattice vibrations characterized by the optical phonon frequencies causes a modulation  $\delta J_i(t)$  of Heisenberg coupling constants due to the periodic change of the hopping matrix elements. From this mechanism we can conclude that the pulse shape of the optical pulse does not enter the driving term, and the optical fs pulse can be treated as instantaneous compared to the phonon and magnon frequencies which are in the small THZ range.

We parameterize the effect of this phonon on the magnetic system by damped oscillations of  $\delta J_i(t)$ . They read in their dimensionless form

$$\frac{\delta J_i(t)}{S J_1^{(0)}} = a_i(t) = a_{0,i} \exp(-\gamma t) \cos(\omega_0 t), \quad (21)$$

where  $a_{0,i} = \delta J_i(0)/J_1^{(0)} = (J_i/J_1^{(0)})\kappa_i$ . In the last step, we introduce the relative change

$$\kappa_i = \delta J_i(0)/J_i^{(0)} \quad (22)$$

while the ratio  $(J_i/J_1^{(0)})$  links  $a_{0,i}$  to the parameters of the equilibrium Hamiltonian. Note that the driving field for the magnon dynamics is governed by the coherent lattice oscillations [28] and not by the time scale of the optical laser pulse.

Once the equilibrium parameters are fixed, the perturbation amplitude is uniquely parameterized by  $\kappa_i$ . The assumption that expression (21) describes the modulation of the exchange coupling is based on the results of previous calculations for a related model in which the phonon dynamics has been computed explicitly [29]. Of course, Eq. (21) represents a simplification, but it is

a reasonable one for small spin-phonon coupling. Moreover, it contains two main ingredients: the amplitude  $a_{0,2}$  and the relaxation rate  $\gamma$  of the modulation. In the following, we focus on the effect of  $\delta J_3(t)$  and omit the index  $i$  therefore. In Sec. IV B, we come back to modulations of  $\delta J_1(t)$  and  $\delta J_2(t)$ .

Describing the oscillations of the coupling by  $\cos(\omega_0 t)$  is consistent with the displacive excitation mechanism of the lattice modes [32]. We access the time dependent sublattice magnetization  $L(t)$  in Eq. (17) by the expectation values of the magnon occupation

$$u_{\vec{k}} := \langle n_{\vec{k}} \rangle = \langle b_{\vec{k}}^\dagger b_{\vec{k}} \rangle \quad (23a)$$

and of the real and imaginary part of the off-diagonal term  $\langle b_{\vec{k}}^\dagger b_{-\vec{k}}^\dagger \rangle$

$$v_{\vec{k}} := \text{Re} \langle b_{\vec{k}}^\dagger b_{-\vec{k}}^\dagger \rangle \quad (23b)$$

$$w_{\vec{k}} := \text{Im} \langle b_{\vec{k}}^\dagger b_{-\vec{k}}^\dagger \rangle. \quad (23c)$$

whose dynamics are calculated by means of Heisenberg's equation  $\frac{dA}{dt} = i\langle [H(t), A] \rangle$ . Since the Hamiltonian does not break translational invariance even in presence of the driving the resulting differential equations

$$\frac{du_{\vec{k}}}{dt} = 2a(t)\beta_{\vec{k}}w_{\vec{k}} - \gamma_r u_{\vec{k}} \quad (24a)$$

$$\frac{dv_{\vec{k}}}{dt} = -2(\omega_{\vec{k}} + a(t)\alpha_{\vec{k}})w_{\vec{k}} - \gamma_r v_{\vec{k}} \quad (24b)$$

$$\begin{aligned} \frac{dw_{\vec{k}}}{dt} &= 2(\omega_{\vec{k}} + a(t)\alpha_{\vec{k}})v_{\vec{k}} + 2a(t)\beta_{\vec{k}}(u_{\vec{k}} + 1/2) \\ &\quad - \gamma_r w_{\vec{k}}, \end{aligned} \quad (24c)$$

do not couple different  $\vec{k}$ -values. But all of them contribute to the collective sublattice magnetization in (17).

In addition to the unitary dynamics induced by the Hamiltonian in the Heisenberg equations of motion we introduce a phenomenological relaxation rate  $\gamma_r$  describing the decay of magnons. By this parameter we quantify the coupling to thermal bath, i.e., we treat the driven spin system as open quantum system and describe it by a Lindblad equation [38] where the creation and annihilation operators of the magnons serve as Lindblad operators [29]. For simplicity, no  $\vec{k}$ -dependence of the relaxation rate  $\gamma_r$  is taken into account.

We solve the set of differential equations for a mesh of  $M$  discrete values  $k_c$  and a mesh of  $M$  discrete frequencies for the density-of-states of the triangular lattice as computed analytically [37]. Note that we absorb the factor  $\hbar$  into the definition of time  $t$  as measured in units of the inverse energy  $1/J_1$ . The numerical results presented in the next sections are obtained by solving the equations (24a)-(24c) with a Bulirsch-Stoer algorithm [39] with 1000 time steps per picosecond. We discretize the Brillouin zone in

$c$ -direction. For the Mn-planes parallel to the  $ab$ -plane, we use the density of states for a triangular lattice [37]. Since we treat the system prior to any pumping to be at zero temperature at equilibrium, we use the initial conditions  $u_{\vec{k}}(t=0) = v_{\vec{k}}(t=0) = w_{\vec{k}}(t=0) = 0$ .

### B. Dynamics of specific magnon modes

Before addressing the total sublattice magnetization we analyze the differential equations of Eq. (24) to understand the dynamics of the expectation values for a single  $\vec{k}$ -mode. If the driving term  $a(t)$  and the relaxation  $\gamma_r = 0$  are set to 0, the magnon occupation does not change

$$\frac{du_{\vec{k}}(t)}{dt} = 0 \Rightarrow u_{\vec{k}}(t) = \text{const.} \quad (25)$$

and  $v_{\vec{k}}$  and  $w_{\vec{k}}$  describe a coherent oscillation between the real and imaginary part of the expectation value  $\langle b_{\vec{k}}^\dagger b_{-\vec{k}}^\dagger \rangle$

$$v_{\vec{k}}(t) = c_0 \cos(2\omega_{\vec{k}} t + \varphi) \quad (26a)$$

$$w_{\vec{k}}(t) = c_0 \sin(2\omega_{\vec{k}} t + \varphi). \quad (26b)$$

with frequency  $2\omega_{\vec{k}}$ . The values of  $c_0$  and  $\delta$  depend on the initial conditions. Clearly, in absence of a damping mechanism once excited the amplitude of coherent oscillations, i. e.,  $|\langle b_{\vec{k}}^\dagger b_{-\vec{k}}^\dagger \rangle|$  does not change in time. If we include a finite damping ( $\gamma_r > 0$ ) the coherent oscillation is damped by the factor  $\exp(-\gamma_r t)$ .

The non-equilibrium dynamics of  $\delta L$  given in Eq. (17) results from the superposition of the contributions of all  $\vec{k}$ -points leading to a decay of the sublattice magnetization due to dephasing. This dephasing results from the differing frequencies  $2\omega_{\vec{k}}$ . The contributing range of these frequencies is  $2\omega_{\text{max}}$  and thus  $1/2\omega_{\text{max}}$  is an estimate for the time scale of this dephasing.

In the presence of the driving term ( $a_0 \neq 0$ ) the differential equations contain the source term  $a(t)\beta_{\vec{k}}$  originating from the two-magnon creation term in the time-dependent part of the Hamiltonian given in Eq. (19). This source term drives the system away from the fixed point  $u_{\vec{k}}(t) = v_{\vec{k}}(t) = w_{\vec{k}}(t) = 0$ . The first term in Eq. (19) is responsible for a modulation of the oscillation frequency by  $2a(t)\alpha_{\vec{k}}$ , i.e.,  $2\omega_{\vec{k}} \rightarrow 2\omega_{\vec{k}} + 2a(t)\alpha_{\vec{k}}$ . But since  $\omega_{\vec{k}}$  dominates over  $a(t)\alpha_{\vec{k}}$  this modulation is often not a sizable effect, see also below.

After the driving term  $a(t)$  has essentially vanished due to its exponential damping, the pair creation stops and  $u_{\vec{k}}(t)$  approaches a constant finite value if we neglect the relaxation ( $\gamma_r = 0$ ). Then the coherent oscillations between  $v_{\vec{k}}$  and  $w_{\vec{k}}$  with a frequency  $2\omega_{\vec{k}}$  occur for large times  $t \gg 1/\gamma$ .

A detailed analytical, approximate evaluation can be found in Appendix A. After recombining,  $z_{\vec{k}}(t) = \langle b_{\vec{k}}^\dagger b_{-\vec{k}}^\dagger \rangle = v_{\vec{k}}(t) + iw_{\vec{k}}(t)$ , we obtain

$$z_{\vec{k}}(t) = ia_0\beta_{\vec{k}} \left[ \frac{e^{-\gamma t}(\omega_0 \sin(\omega_0 t) - (2i\omega_{\vec{k}} + \gamma - \gamma_r) \cos(\omega_0 t))}{\omega_0^2 - (2\omega_{\vec{k}} - i(\gamma - \gamma_r))^2} + \frac{(2i\omega_{\vec{k}} + \gamma - \gamma_r)e^{2i\omega_{\vec{k}} t} e^{-\gamma_r t}}{\omega_0^2 - (2\omega_{\vec{k}} - i(\gamma - \gamma_r))^2} \right] \quad (27)$$

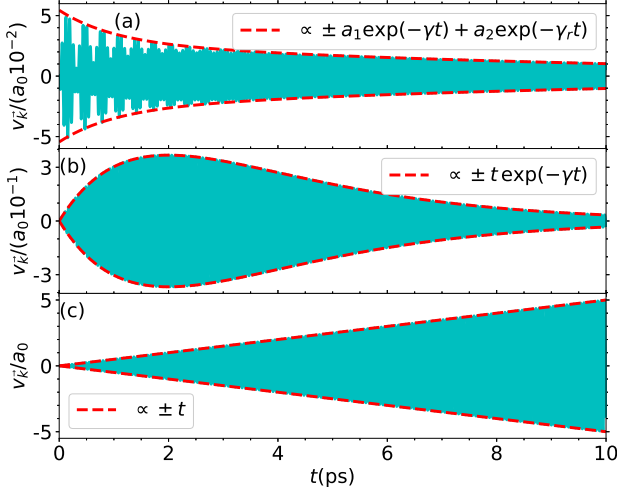


FIG. 3. The analytic solution  $v_{\vec{k}}(t)$  according to Eq. (27) for off-resonant driving and Eq. (28) for resonant driving, respectively. (a) Off-resonant driving with  $\omega_0 = 80 \text{ ps}^{-1}$ ,  $\omega_{\vec{k}} = 50 \text{ ps}^{-1}$ ,  $\gamma = 1.0 \text{ ps}^{-1}$ , and  $\gamma_r = 0.1 \text{ ps}^{-1}$ . Resonant driving for  $2\omega_{\vec{k}} = \omega_0 = 100 \text{ ps}^{-1}$  with (b)  $\gamma = \gamma_r = 0.5 \text{ ps}^{-1}$  and (c)  $\gamma = \gamma_r = 0$  (Parameters:  $\kappa = 0.01, \beta_{\vec{k}} = 1$ ).

which enters Eq. (24a).

Resonantly driven modes, i.e., modes for which  $\omega_0^2 \approx (2\omega_{\vec{k}})^2$  holds, acquire a large amplitude and contribute the most to  $\delta L$ . The first term on the right hand side of Eq. (27) describes the coherent oscillations with driving frequency  $\omega_0$  and an exponential envelope decreasing with the rate  $\gamma$ . The second term includes the oscillations with twice the eigen frequency  $\omega_{\vec{k}}$  of each  $\vec{k}$ -mode. The factor of two stems from the fact that magnons are created in pairs with total momentum zero and at  $\vec{k}$  and  $-\vec{k}$ , both of which have the same frequency  $\omega_{\vec{k}} = \omega_{-\vec{k}}$ . In addition, the second term decays exponentially with decay rate  $\gamma_r$ . For zero relaxation of the magnon,  $\gamma_r = 0$ , the amplitude of the second term is constant.

Figure 3(a) shows this general behavior for off-resonant driving with  $\omega_0 = 100 \text{ ps}^{-1}$ ,  $\omega_{\vec{k}} = 80 \text{ ps}^{-1}$ ,  $\gamma = 1.0 \text{ ps}^{-1}$ , and  $\gamma_r = 0.1 \text{ ps}^{-1}$  as cyan line. The envelope is plotted as dashed red line; it is the superposition of the two decays determined by  $\gamma$  and  $\gamma_r$ .

From Eq. (27) we read off that  $v_{\vec{k}}(t)$  and  $w_{\vec{k}}(t)$  depend linearly on the driving amplitude  $a_0$  in leading order and that  $v_{\vec{k}}(t)$  and  $w_{\vec{k}}(t)$  being real and imaginary part of  $\langle b_{\vec{k}}^\dagger b_{-\vec{k}}^\dagger \rangle$  are related by a phase shift of  $\pi/2$ . Substituting the solution for  $w_{\vec{k}}(t)$  into Eq. (24a) reveals that  $u_{\vec{k}}(t) \propto a_0^2$  in lowest order.

The denominator in Eq. (27) vanishes for resonant

driving  $\omega_0 = 2\omega_{\vec{k}}$  and the special choice  $\gamma = \gamma_r$ . A closer inspection reveals that this is a removable singularity without physical significance: Considering the limit  $\omega_0 \rightarrow 2\omega_{\vec{k}}$  properly we obtain

$$z_{\vec{k}}(t) = \frac{ia_0\beta_{\vec{k}}}{2} e^{-\gamma t} \left( t e^{i\omega_0 t} + \frac{1}{\omega_0} \sin(\omega_0 t) \right). \quad (28)$$

As known from resonant driving of harmonic oscillators, the amplitude increases linearly as a result of the secular term. In presence of damping, the exponential decay sets in at later times.

Figure 3(b) illustrates the envelope of the resonantly driven system at  $\gamma = \gamma_r = 0.5 \text{ ps}^{-1}$ . The envelope is given approximately by  $\propto t \exp(-\gamma t)$  as expected from Eq. (28). For  $\gamma = \gamma_r = 0$ , we indeed obtain a linearly increasing amplitude as shown in Fig. 3(c).

On the basis of experimental findings for  $\alpha$ -MnTe [23], we assume that the relaxation rate  $\gamma_r$  is significantly smaller than the damping rate  $\gamma$  of the driving term. Consequently, the effect of the decay of the magnon occupation happens on time scales much longer than the duration of the driving pulse. This is also the justification to introduce this decay in a phenomenological way. It is the slowest effect and thus can be described by a Lindbladian dynamics.

The contribution of resonantly driven  $\vec{k}$ -modes to  $\delta L$  is especially large. Hence, we want to understand their dynamics in particular. For simplicity, we set  $\gamma_r = 0$  which is justified for short and intermediate time scales where  $\gamma_r t \ll 1$ . First, we consider a driving term with constant amplitude. For this case, we are able to perform a more comprehensive analytical calculations than the one presented in Eq. (27) by adapting the approach in Ref. [29]. We take the terms  $a(t)\alpha_{\vec{k}}$  and  $u_{\vec{k}}$  in the integral in Eq. (A4) into account.

We focus on the slow change of  $u_{\vec{k}}$  only, i.e., we average out the fast oscillations at frequencies  $\omega_0$  and  $2\omega_0$ . This is done by averaging over  $T_0 = \frac{2\pi}{\omega_0}$ , for details see App. B1. We distinguish between resonant driving and two types of off-resonant driving. At the resonance condition  $2\omega_{\vec{k}} = \omega_0$ , the magnon occupation increases in time without limit

$$u_{\vec{k}}(t) = \frac{1}{2} (\cosh(\Gamma t) - 1) \quad (29a)$$

with

$$\Gamma := \frac{\beta_{\vec{k}}\omega_0}{\alpha_{\vec{k}}} J_1 \left( \frac{2a_0\alpha_{\vec{k}}}{\omega_0} \right) \approx a_0\beta_{\vec{k}}. \quad (29b)$$

Here,  $J_1(x)$  denotes the Bessel function of the first kind. For numbers that are typically present in the experiment we can approximate it by its linear term in the Taylor series for small argument.

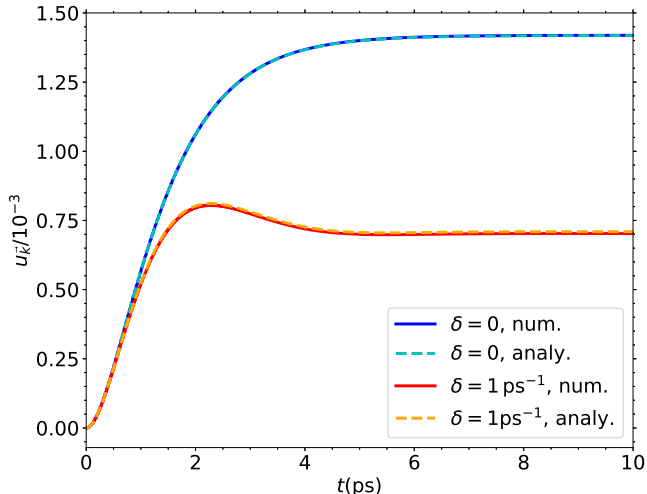


FIG. 4. The magnon occupation  $u_{\vec{k}}(t)$  of a specific magnon mode  $\omega_{\vec{k}} = 50 \text{ ps}^{-1}$  for damped resonant (dark and light blue) and damped off-resonant (red and orange) driving  $\delta = 1 \text{ ps}^{-1}$ . The solid curves represent the full numerical solution while the dashed curves represent the analytical approximations Eqs. (31) and (32) with  $\kappa = 0.01, \beta_{\vec{k}} = 1, \Gamma = 0.0753 \text{ ps}^{-1}, \Gamma' = 0.9972 \text{ ps}^{-1}$ .

For a driving frequencies slightly off-resonance with a finite detuning  $\delta = 2\omega - \omega_0$ , we have to distinguish between two cases depending on whether the detuning is smaller (a) or larger (b) than the energy scale of pumping  $\Gamma$

(A)  $\Gamma > |\delta|$

$$u_{\vec{k}}(t) = \frac{1}{2} \frac{\Gamma^2}{\Gamma'^2} (\cosh(\Gamma't) - 1) \quad (30a)$$

$$\text{with } \Gamma' := \sqrt{|\Gamma^2 - \delta^2|} \quad (30b)$$

(B)  $\Gamma < |\delta|$

$$u_{\vec{k}}(t) = \frac{1}{2} \frac{\Gamma^2}{\Gamma'^2} (1 - \cos(\Gamma't)). \quad (30c)$$

Figure 4 illustrates the numerical results if the driving term is no longer constant, but damped with  $\gamma = 1 \text{ ps}^{-1}$ . The figure shows the numerically computed dynamics of the same  $\vec{k}$ -mode for resonant (blue solid curve) and off-resonant driving (red solid curve). The numerical solution contains fast oscillations at frequency  $2\omega_0$ . Since the amplitudes are very small, these oscillations are not visible in the figure. However, Fig. 15b shows them analogously for the case  $\gamma = 0$ . Due to the finite phonon oscillation duration  $\approx 1/\gamma$  the magnon occupation does not grow beyond any limit as for indefinite driving, but saturates. This behavior applies to the case of resonant and for detuned driving.

We extend the derivation of the slowly varying contribution to  $u_{\vec{k}}$  to the case where the displacement oscillation has an exponential decaying envelope, see App. B 2. This case, however, is more subtle than the previous case so that an analytical derivation is only possible in leading order of  $a_0$ , so that we henceforth use  $\Gamma = a_0\beta_{\vec{k}}$ , cf. Eq. (29b). This assumption allows us to derive a differential equation for the slowly varying part of  $u_{\vec{k}}$ , see App. B 2. But, unfortunately no closed analytical expression for its solution could be found. If we assume that the values of  $u_{\vec{k}}$  are such that they fulfill  $2u_{\vec{k}} \ll 1$  we can establish

$$u_{\vec{k}}(t) = \frac{\Gamma^2}{4\gamma^2} (1 - \exp(-\gamma t))^2 \xrightarrow{t \rightarrow \infty} \frac{\Gamma^2}{4\gamma^2} \quad (31)$$

for the resonant case and for the detuned case

$$u_{\vec{k}}(t) = \frac{\Gamma^2}{4(\gamma^2 + \delta^2)} |\exp(i\delta t) - \exp(-\gamma t)|^2 \quad (32a)$$

$$\xrightarrow{t \rightarrow \infty} \frac{\Gamma^2}{4(\gamma^2 + \delta^2)} \quad (32b)$$

for small detuning  $|\delta| \ll \omega_0$ . Both show that  $u_{\vec{k}}$  saturates to a finite value because we do not consider magnon relaxation  $\gamma_r$  in this analysis. To neglect  $\gamma_r$  in the analysis for short time scales is justified because its effect generically sets in on longer time scales. Note that the saturation value is not necessarily reached monotonically in the case of finite detuning, see Fig. 4(a). It is interesting that slow oscillations with the frequency given by the detuning occur.

### C. Pulse induced changes of sublattice magnetization

The effect of the driving laser pulse is characterized by three parameters in Eq. (21). The parameter  $a_0$  determines the oscillation strength induced by the coherent optical phonon at frequency  $\omega_0$  which has been excited by the laser. It is damped by the relaxation rate  $\gamma$ . Here we do not yet consider the long-time decay due to the relaxation rate  $\gamma_r$ . In the next three sections, We analyze the effect of each of these parameters on the changes of the sublattice magnetization  $\delta L(t)$  introduced in Eq. (17).

In Fig. 5, two generic curves are depicted for the same  $\gamma$  and amplitude  $a_0$ , but different driving frequencies  $\omega_0$ . No relaxation  $\gamma_r$  has been considered here. Coherent oscillations occur at the driving frequency. The envelope function consists of fast building while the driving field is active and a consecutive slow decay. For the faster driving frequency  $\omega_0$  a build-up phase and a more complex decay pattern is observed. For the lower driving frequency, we are able to fit an exponential envelope function with a decay rate of  $c_1 = 1.2(3) \text{ ps}^{-1}$  displayed as dashed blue line in Fig. 5.

The change of the sublattice magnetization saturates at a finite value  $\delta L(t \rightarrow \infty)$  which can be calculated by

$$\delta L_{\infty} = \lim_{T \rightarrow \infty} \frac{1}{T} \int_0^T \delta L(t). \quad (33)$$



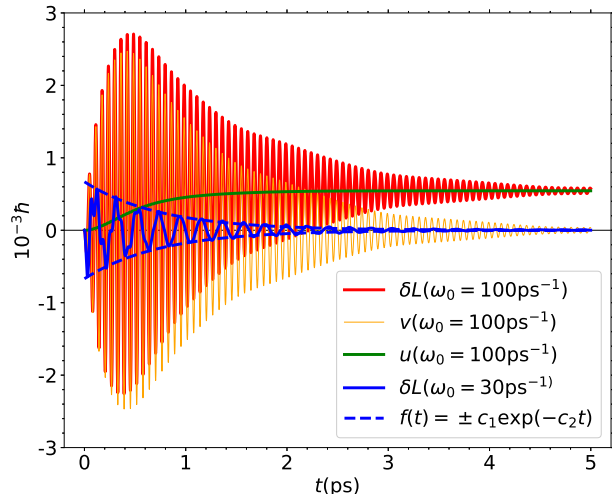


FIG. 5. The change of the sublattice magnetization oscillates in time depending on the parameters of driving: the strength of driving  $a_0$ , the damping  $\gamma$ , and the driving frequency  $\omega_0$ . The curves are computed for  $\kappa = 0.01$ ,  $\gamma = 1.0 \text{ ps}^{-1}$ . An envelope of the amplitude can be fitted  $f(t) = \pm c_1 \exp(-c_2 t)$  with  $c_1 = 6.7(1) \times 10^{-4}$ ,  $c_2 = 1.34(5) \text{ ps}^{-1}$ . Exemplarily, the two main contributions of  $\delta L$  are shown for  $\omega_0 = 100 \text{ ps}^{-1}$  (red curve), see Eqs. (17) and (23). The slowly evolving contribution (green curve) consists of the magnon occupation  $u_{\vec{k}}$  summed over all  $\vec{k}$ -modes in Eq. (34a). The oscillating part consists of the summed contributions  $v_{\vec{k}}$  in Eq. (34b) (orange curve) (Parameter:  $M = 1000$ ,  $\gamma_r = 0$ ).

In order to distinguish qualitatively different contributions to  $\delta L$ , we plot the slowly varying contribution  $u(t)$  and the oscillating one  $v(t)$  defined by

$$u(t) = \sum_{\vec{k}} \frac{A_{\vec{k}}}{\omega_{\vec{k}}} u_{\vec{k}}, \quad (34a)$$

$$v(t) = \sum_{\vec{k}} \frac{B_{\vec{k}}}{\omega_{\vec{k}}} v_{\vec{k}} \quad (34b)$$

in Fig. 5. The saturation value  $\delta L_{\infty}$  is determined by the long-time values of the magnon occupations since the oscillating contribution of  $v_{\vec{k}}$  in Eq. (17) averages out and vanishes due to dephasing.

The sum of all magnon occupations  $u_{\vec{k}}(t)$  is always positive and reaches a finite value for large times after a single laser pulse. As a result, the change of the sublattice magnetization approaches a finite value as well. Since we have neglected interactions between different  $\vec{k}$ -modes the constant saturation cannot decay. In experiments, however, slow relaxation processes induce a slow decay of  $\delta L_{\infty} \rightarrow 0$  requiring to include an additional phenomenological relaxation rate  $\gamma_r$ , see below.

### 1. Dependence on the driving amplitude

The response of the sublattice magnetization increases with increasing amplitude  $a_0$  of the driving. For a quantitative measure, we extracted the absolute maximum of  $|\delta L(t)|$ , denoted  $\max|\delta L|$ , and plotted it versus  $\kappa$  for two driving frequencies  $\omega_0$  in Fig. 6. The symbols represent the values of the numerical simulations while the solid lines are first and second order fits, respectively.

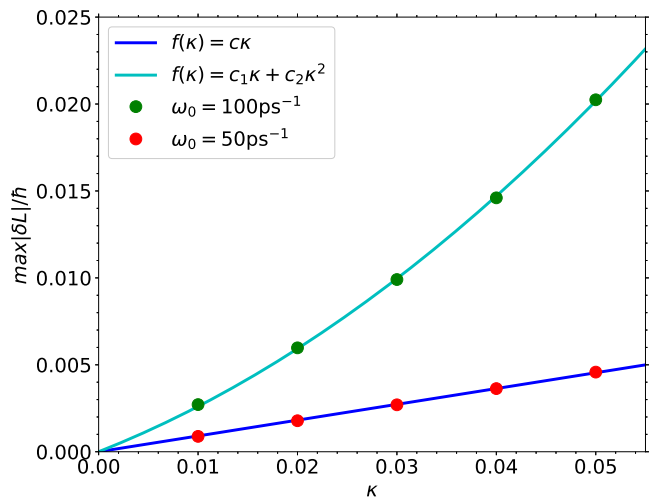


FIG. 6. The maximum value of  $|\delta L|$  depends linearly on the relative amplitude  $\kappa$  of the driving, see Eq. (22), if the driving is small enough. Generally, non-linear contributions are also important. Parameters:  $\gamma = 1.0 \text{ ps}^{-1}$ ,  $M = 100$ ,  $c = 0.0909(4)$ ,  $c_1 = 3.6(1)$ ,  $c_2 = 0.225(6)$ .

According to Eq. (17),  $\delta L(t)$  consists of two contributions: the driving induced the magnon occupations  $u_{\vec{k}} = \langle n_{\vec{k}} \rangle$  and the major oscillatory part given by the sum over all  $v_{\vec{k}} = \Re \langle b_{\vec{k}}^{\dagger} b_{\vec{k}} \rangle$ . While the contribution stemming from all  $u_{\vec{k}}$  is small and mainly determines  $\delta L_{\infty}$ ,  $|\delta L(t)|$  is strongly influenced by  $v_{\vec{k}}$ .

In order to study the dependence on  $a_0$  in leading order, we inspect the differential equations (24a)-(24c). For very small magnon occupations,  $u_{\vec{k}} \ll 1$ , one finds  $v_{\vec{k}}, w_{\vec{k}} \propto a_0$  from Eq. (23c) and, consequently,  $u_{\vec{k}} \propto a_0^2$  through Eq. (23a). Therefore, we expect a parabolic fit  $c_1 a_0 + c_2 a_0^2$  describing the  $a_0$  dependency of  $\max|\delta L|$  very accurately, as demonstrated by the solid lines in Fig. 6. We can fit the  $\max|\delta L|$  dependence on  $a_0$  with  $ca_0$  for  $\omega_0 = 50 \text{ ps}^{-1}$ ,  $\gamma = 1.0 \text{ ps}^{-1}$ , with  $c = 0.0909(4)$ , and added the fit curve as solid blue line in Fig. 6. For  $\omega_0 = 100 \text{ ps}^{-1}$ , a parabolic fit  $c_1 a_0 + c_2 a_0^2$  is needed with  $c_1 = 3.5(1)$ ,  $c_2 = 0.225(6)$ ; it is added as cyan solid lines confirming our analysis of Eq. (24).

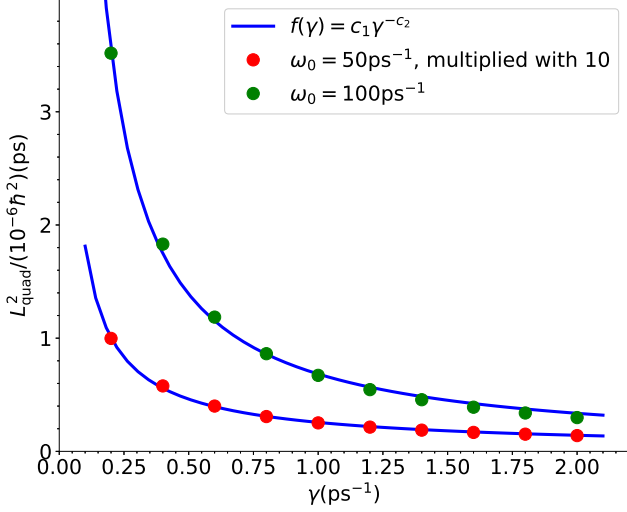


FIG. 7. The value  $L_{\text{quad}}^2$  decreases for increasing decay rate  $\gamma$  of the driving term roughly like  $1/\gamma$ . The data for  $\omega_0 = 50 \text{ ps}^{-1}$  is multiplied by 10 for better visibility. The fit parameters are  $c_2 = 0.850 \pm 0.009$  for  $\omega_0 = 50 \text{ ps}^{-1}$  and  $c_2 = 1.02 \pm 0.01$  for  $\omega_0 = 100 \text{ ps}^{-1}$  (Parameter:  $M = 100, \kappa = 0.005$ .)

## 2. Dependence on the driving duration

The driving duration  $\propto 1/\gamma$  is parameterized by the decay rate  $\gamma$  of the coherent phonon mode responsible for the periodic modulation of  $\delta J_3(t)$  as stated in Eq. (21). In order to quantify the total effect of the fluctuating part of the sublattice magnetization relative to the steady state we define

$$L_{\text{quad}}^2 := \int_0^\infty (\delta L(t) - \delta L_\infty)^2 dt. \quad (35)$$

Note that we deduct the saturation value  $\delta L_\infty$  in order to ensure convergence of the integral in spite of its infinite upper limit. So the quantity  $L_{\text{quad}}^2$  measures in particular the oscillatory part of  $\delta L$ .

In Fig. 7, the data points for  $L_{\text{quad}}$  are depicted as colored dots as function of  $\gamma$  for two frequencies  $\omega_0$  and a fixed driving amplitude  $a_0$ . The solid lines are fits of the form

$$f(\gamma) = c_1 \gamma^{-c_2} \quad (36)$$

with an exponent  $c_2 \approx 1$ . The simulated data and the fits with exponents of about 1 agree quite well. Since the duration of the displacement oscillation is  $\propto 1/\gamma$  this result reflects the fact that the response of the system grows proportional to the time the driving is applied. This makes sense since the amount of energy which can be deposited by the oscillating phonon grows linearly with the time it lasts.

Since we subtract the long-time saturation value  $\delta L_\infty$  governed by the sum over magnon occupations  $u_{\vec{k}}$  in

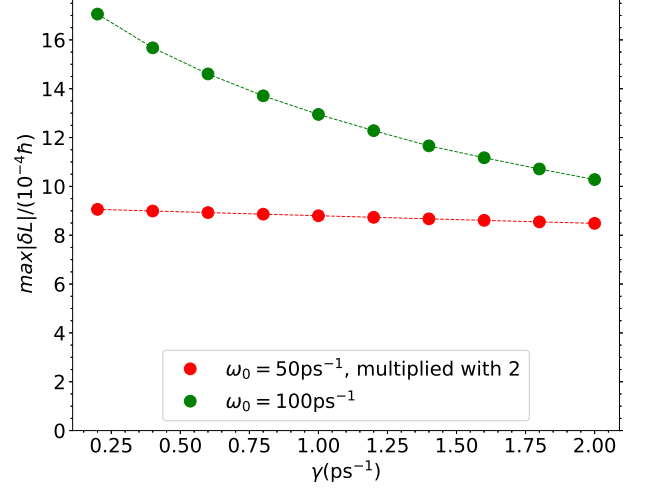


FIG. 8.  $\max|\delta L|$  vs the damping rate  $\gamma$  for two values of  $\omega_0$ . The data for  $\omega_0 = 50 \text{ ps}^{-1}$  is multiplied by 2 for better visibility. (Parameter:  $M = 100, \kappa = 0.005$ .)

Eq.(35),  $L_{\text{quad}}^2$  is mainly sensitive to the two-magnon off-diagonal expectation value  $v_{\vec{k}}$ . Some analytic insight into the dynamics of the full problem can be gained by our approximate solution for  $v_{\vec{k}}(t)$  stated in Eq. (27). Since the time-dependent parts in Eq. (27) only depend on the magnon energy  $\omega_{\vec{k}}$  one can define an auxiliary effective DOS  $\tilde{\rho}(\omega)$ ,

$$\tilde{\rho}(\omega) = \frac{1}{N\omega} \sum_{\vec{k}} \beta_{\vec{k}} B_{\vec{k}} \delta(\omega - \omega_{\vec{k}})$$

to convert the  $k$ -summation in Eq. (17) for the  $v_{\vec{k}}(t)$  contribution into a integration over frequency. The resonantly driven magnons contribute the most to the integral: Since the amplitude is proportional to  $1/\gamma$  and the width in frequency of the modes with the highest amplitude is proportional to  $\gamma$ , the overall  $\gamma$  dependency cancels out in  $(\delta L(t) - \delta L_\infty)$  This is clearly shown in Fig. 8 where one can discern that the maximum of  $\delta L$  depends only very weakly on  $\gamma$  especially for smaller  $\omega_0$ . Then we are left with exponential decay of  $v_{\vec{k}}(t)$  with rate  $\gamma$  implying that the magnetic response lasts for about  $1/\gamma$ , see Sect. III C 4. Due to the integration in Eq. (35) this implies  $L_{\text{quad}}^2 \propto 1/\gamma$  as demonstrated in Fig. 7.

## 3. Dependence on the driving frequency $\omega_0$

Fig. 5 already shows that the change of the sublattice magnetization strongly depends on the driving frequency  $\omega_0$  for the same driving amplitude  $a_0$  and driving decay  $\gamma$ . For fixed  $a_0$  and  $\gamma$  we scan the driving frequency  $\omega_0$  and extract  $\max|\delta L|$  as well as the saturation value  $\delta L_\infty$ . The generic results of this scan are depicted in Fig. 9.

Even though the sublattice magnetization and all related quantities are sums over all  $\vec{k}$ -modes it is obvious

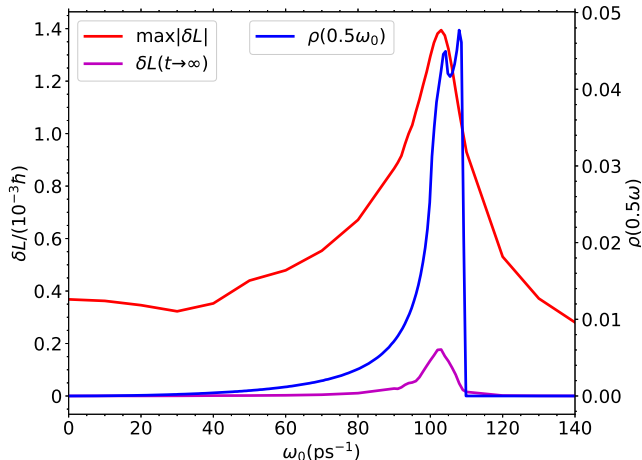


FIG. 9. The maximum value of  $|\delta L|$  and the saturation value  $\delta L(t \rightarrow \infty)$  show a behavior similar to the magnon DOS except for a factor 2 in the frequency because of the resonance condition  $2\omega_{\vec{k}} \approx \omega_0$ . ( $M = 100, \kappa = 0.005, \gamma = 1 \text{ ps}^{-1}$ ).

that the modes in resonance or very close to it contribute that most to  $\delta L$ . Hence, one expects that the response of  $\delta L$  follows roughly the DOS of the magnons because a high density of modes with  $2\omega_{\vec{k}} \approx \omega_0$  is favorable for a strong effect in  $\delta L$ . As this argument implies there is a factor of 2 between the DOS and the behavior of  $\delta L$  because the resonance condition holds for pairs of magnons. Indeed, Fig. 9 clearly illustrates that these ideas are correct, at least on a qualitative level. As expected,  $\max|\delta L|$  and  $\delta L_\infty$  peak at the van-Hove singularities of the magnon DOS.

Interestingly, the saturation value  $\max|\delta L|$  becomes significant only in the vicinity of the peaks of the van-Hove singularities while  $\max|\delta L|$  acquires significant values also away from the prominent peaks of the DOS. We attribute this to the fact that saturation value is large only at or close to resonance, see Eq. (32). A mode is far from resonance if  $|\delta| \gg \gamma$  which is the case for most modes in view of the typical small values of  $\gamma$ . In contrast,  $\max|\delta L|$  depends on the oscillatory contributions of all modes at small or moderate times, see Eq. (27). Hence it does not depend so strongly on the DOS of magnons.

#### 4. Long-time decay of the change of the sublattice magnetization

We still consider the physical situation without phenomenological magnon decay, i.e., for  $\gamma_r = 0$ . Still, the change of the sublattice magnetization does decay in seeming contrast to the dynamics of single modes. The decay of  $\delta L$  in time results from dephasing, i.e., from the fact that all  $\vec{k}$ -modes contribute but they display oscillations with a broad range of frequencies which quickly become out-of-phase so that the signal decreases. The

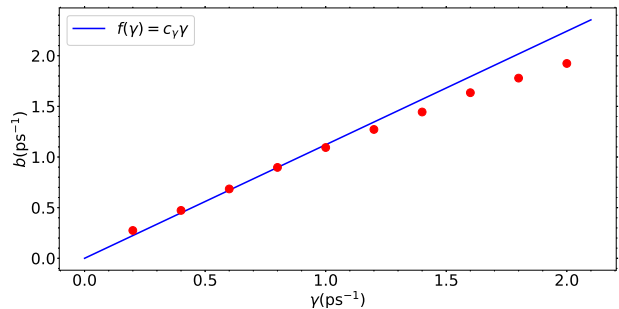


FIG. 10. Effective dephasing rate  $b$  of the envelope of oscillatory part of the sublattice magnetization as function of the decay rate of the driving force. For small  $\gamma$  the relation is linear as expected in the limit where the actual dephasing rate is very large, see main text. The prefactor is of the order of unity  $c_\gamma = 1.12(2)$ . ( $M = 100, \kappa = 0.005, \omega_0 = 30 \text{ ps}^{-1}$ )

time scale on which this dephasing takes place is roughly estimated by  $\tau_{\text{dephas}} \approx 1/(2\omega_{\text{max}})$  where  $\omega_{\text{max}}$  is the maximum frequency of the magnon dispersion and the factor 2 stems from the fact that pairs of magnons are created. In generic experimental set ups,  $\tau_{\text{dephas}}$  is much smaller than the displacement oscillation duration  $1/\gamma$  so that the signal dies out extremely fast once the driving oscillation disappeared. In turn, this implies that the characteristic time scale on which  $\delta L$  vanishes is expected to be proportional to the duration of the driving term.

We want to put this hypothesis to test. As shown in Fig. 5,  $\delta L(t)$  approaches a finite saturation value  $\delta L_\infty$  for  $\gamma_r = 0$  while the oscillatory part decays in time. We separate the oscillatory part of  $\delta L$  and fit its envelope by an exponential

$$e(t) = ce^{-b(\gamma)t} \quad (37)$$

from which we read off the effective dephasing rate  $b(\gamma)$ . The resulting values are displayed in Fig. 10 as function of  $\gamma$ . We stress that this analysis was done for a relatively small driving frequency  $\omega_0 = 30 \text{ ps}^{-1}$  which is far away from the van-Hove singularities where the two peaks in the DOS introduce an additional time dependence as shown by the red curve in Fig. 5. Then a mono-exponential analysis of the characteristic dephasing rate is not possible.

For a frequency in the featureless range of the magnon DOS we find our hypothesis supported in Fig. 10 displaying a linear dependence  $b \propto \gamma$ . This means that the time scale of the decay of the oscillations in  $\delta L$  is dominated by the time scale of the driving oscillation duration. Note that the proportionality factor  $c_\gamma$  is about unity so that both time scales coincide the regime of small  $\gamma$ . Only for larger values of  $\gamma$  some downward curvature appears. This feature is not unexpected either because for  $\gamma \rightarrow \infty$  one expects that the limiting process of signal decay is the dephasing on the time scale  $1/(2\omega_{\text{max}})$  so that  $b(\gamma)$  saturates at some value  $b_\infty = \lim_{\gamma \rightarrow \infty} (b(\gamma))$  of the order of  $2\omega_{\text{max}}$ .

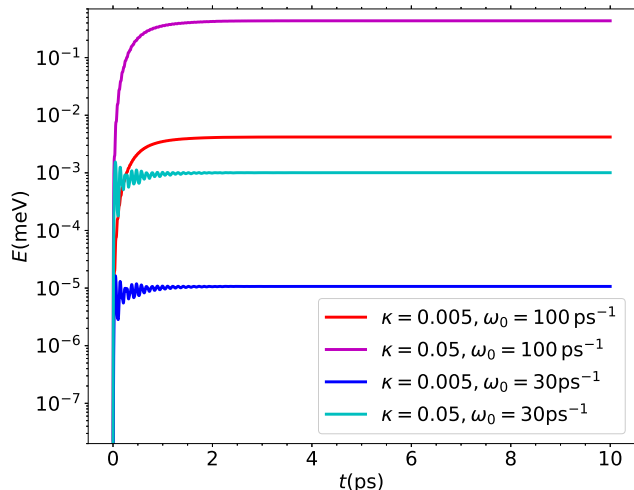


FIG. 11. The energy per site  $E(t)$  for different combinations of  $\kappa$  and  $\omega_0$ . The energy reaches a saturation value for  $t \rightarrow \infty$  since the driving oscillation is damped with rate  $\gamma = 1 \text{ ps}^{-1}$ , i.e., the oscillation is effectively of finite duration. All curves start at zero energy since we start from the system at zero temperature. (Parameter:  $M = 100, \gamma_r = 0$ ).

### 5. Time evolution of the total energy

A driven system acquires energy through the driving. So it is an important question how much energy is pumped into it and on which parameters this effect depends. We define the total energy energy  $E$  per spin by

$$E(t) = \frac{1}{N} (\langle H(t) \rangle - J_1 S(E_d + \Delta E)) \quad (38)$$

where  $H(t)$  is given by Eq. (18). In the above definition we subtracted the trivial energy offset of  $H_0$ . While  $E(t)$  initially oscillates and increases on average it reaches a saturated value for times  $t \gg 1/\gamma$  which represents its long-time limit.

Figure 11 depicts the time evolution of  $E(t)$  for two different driving frequencies and two different driving amplitudes in Fig. 11. The saturation value of the energy depends on the driving frequency and the amplitude of the driving. If the resonance condition is fulfilled or almost fulfilled for many of  $\vec{k}$ -modes, quantified by the magnon DOS in Fig. 2(b), the energy uptake is facilitated and higher values of energy are reached. Thus, even a small driving with  $\kappa = 0.005$  leads to a higher excitation if it is done at frequency at the peaks of the DOS than the ten times larger driving at small values of the DOS.

For the stronger driving one can discern oscillations for short times. They are also present for the weaker driving, but much smaller. We presume that the driving at around the DOS maxima leads to substantial contributions from many magnons so that the signal is better averaged and hence does not fluctuate so strongly. The

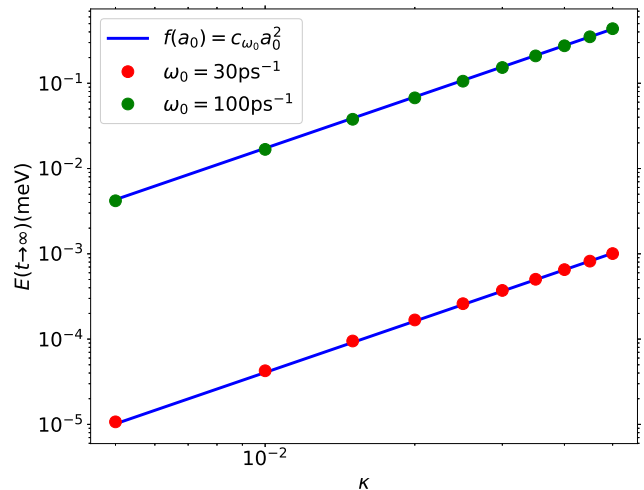


FIG. 12. The saturation value of the energy per site  $E(t \rightarrow \infty)$  depends quadratically on the relative amplitude  $\kappa$  of the driving. The fit parameters are  $c_{\omega_0} = 0.406(1) \text{ ps}^{-1}$  for  $\omega_0 = 30 \text{ ps}^{-1}$  and  $c_{\omega_0} = 173.0(5) \text{ ps}^{-1}$  for  $\omega_0 = 100 \text{ ps}^{-1}$  (Parameter:  $M = 100, \gamma = 1.0 \text{ ps}^{-1}$ ).

amplitude of the oscillation is much smaller than the increasing slowly varying component of  $E(t)$  and, therefore, not visible in the figure.

We already demonstrated in Fig. 9 that the change of the sublattice magnetisation reaches a maximum for  $\omega_0 = 100 \text{ ps}^{-1}$ . Additionally, we selected  $\omega_0 = 30 \text{ ps}^{-1}$ . For both frequencies, we investigate the dependence of the saturation value  $E(t \rightarrow \infty)$  on the driving amplitude  $a_0$ . The data shown in Fig. 12 is perfectly described by  $E(t \rightarrow \infty) \propto a_0^2$ . This could be naively expected in analogy to a driven classically harmonic oscillator where the energy absorption is proportional to the square of the driving amplitude or, alternatively, as direct implication of Fermi's Golden Rule.

Inspecting the details of our calculation, we observed already earlier that  $u_{\vec{k}}$  grows quadratically with  $a_0$ , see the discussion after Eq. (27). It is particularly obvious in the explicit expressions for the saturated limits of  $u_{\vec{k}}$  in Eqs. (31) and (32), we recall  $\Gamma \propto a_0$ . In the long-time limit, the time dependent contribution  $X(t)$  to the Hamiltonian vanishes exponentially  $\propto \exp(-\gamma t)$  so that only  $H_0$  contributes to  $E(t)$  for  $t \rightarrow \infty$ . Consequently, only  $u_{\vec{k}}$  enters in the expectation value according to Eq. (9) and hence this value depends quadratically on the driving amplitude.

## IV. MAKING CONTACT TO EXPERIMENTS

To connect our calculations closer to experiments, we include a finite relaxation rate  $\gamma_r$  that parametrizes relaxation processes beyond the Hamiltonian (1) in an effective Lindblad equation. The reservoir consists of all

the phonons in MnTe.

In addition, we investigate whether decisive qualitative differences occur if the optical phonon couples to the other exchange couplings in the system, namely  $J_1$  or  $J_2$ .

### A. Effect of the magnon relaxation

The linear spin wave theory employed so far neither contains neither any scattering between the magnon modes nor does it contain relaxation terms which allow the system to reach its initial equilibrium again after a long time. In order to provide a theoretical description that includes relaxation back to the initial equilibrium state prior to the photo-excitation, we have already introduced an additional relaxation rate  $\gamma_r$  in Eqs. (24). In this section, we consider a finite value of  $\gamma_r > 0$  explicitly. The derivation of the approximate analytic solution is lengthy, but can be found in App. B3.

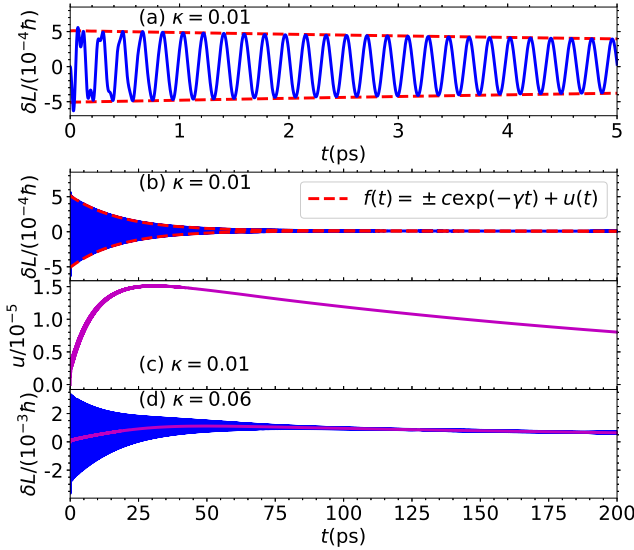


FIG. 13. Evolution of  $\delta L(t)$  including relaxation parametrized by  $\gamma_r = 3.9 \times 10^{-3} \text{ ps}^{-1}$ . The other parameters are also adapted to experiment [23]:  $\omega_0 = 33.6 \text{ ps}^{-1}$ ,  $\gamma = 0.055 \text{ ps}^{-1}$ ,  $M = 2200$ . Panel (a) focuses on the short-time dynamics for  $\kappa = 0.01$  to illustrate the fast oscillations. Panel (b) shows the long-time dynamics. Panel (c) shows the contribution of the slowly varying contribution  $u(t)$  of  $\delta L(t)$  of panel (b) which decays like  $\exp(-\gamma_r t)$ ; note the difference of scales of the  $y$  axes. Panel (d) also displays  $\delta L(t)$  and the slow contribution  $u(t)$ , but for larger relative driving amplitude  $\kappa = 0.06$ .

Figure 13 shows  $\delta L(t)$  and  $u(t)$  for typical experimental driving frequencies and coherent lattice oscillation durations in  $\alpha$ -MnTe [23]. Since the driving amplitude  $a_0$  is unknown, we perform calculations for  $\kappa = 0.01$  and  $\kappa = 0.06$  to illustrate the possible outcomes for smaller and for larger driving amplitude.

Figure 13 shows  $\delta L(t)$  as blue curves. The oscillations of  $\delta L(t)$  are so fast that they can only be resolved on time scale of panel (a). The contribution  $u(t)$  to

$\delta L(t)$  is depicted separately in Fig. 13(b) to illustrate the relaxation due to  $\gamma_r$  visible on the long-time range. For  $\kappa = 0.01$ , the contribution of the magnon occupation is very small compared to the oscillatory contribution  $v(t)$ . Therefore, including an additional magnon relaxation term has only a minor effect on  $\delta L(t)$ . Since  $\gamma = 0.055 \text{ ps}^{-1} > \gamma_r = 3.9 \times 10^{-3} \text{ ps}^{-1}$ , we observe an initial increase of the amplitude due to the driving of the system up to the time scale  $T_d \approx 1/\gamma$  before the decay sets in. Then  $\delta L(t)$  is determined only by  $u(t)$  as discussed above. At the larger time scale,  $t > 1/\gamma_r$ , the magnon occupation  $u(t)$  exponentially decays proportional to  $\exp(-\gamma_r t)$  so that  $\delta L(t)$  vanishes asymptotically for  $t \rightarrow \infty$ .

Figure 13(c) depicts  $\delta L(t)$  for a larger driving amplitude  $\kappa = 0.06$ . In contrast to the results for  $\kappa = 0.01$ ,  $u(t)$  shown as violet curve becomes significantly larger relative to the oscillatory component. This is consistent with the linear dependence of the oscillatory component on the amplitude  $a_0$ , while the slowly varying component grows quadratically in  $a_0$ .

For the realistic parameter regime of  $\gamma > \gamma_r$ , most of the previous analysis of the case at  $\gamma_r = 0$  continues to apply in the presence of  $\gamma_r$ . Especially,  $\max|\delta L|$  does not change significantly if  $\gamma \gg \gamma_r$  since it is dominated by the short-time dynamics hardly affected by a small value of  $\gamma_r$ . Therefore, we do not investigate the effect of  $a_0$  and  $\gamma$  on  $\delta L$  for finite  $\gamma_r$  again. Only the decreasing envelope of the amplitude of  $\delta L$  becomes more complicated, but shows the expected behavior: the mono-exponential decay is replaced by a bi-exponential decay with two decay rates  $\gamma$  and  $\gamma_r$ . The latter determines the behavior for long times. We stress that including  $\gamma_r$ , implies that the dynamic system approaches its fixed point given by  $u_{\vec{k}}(t) = v_{\vec{k}}(t) = w_{\vec{k}}(t) = 0$ . The magnetic energy pumped into the Heisenberg model by the lattice driving is eventually dissipated into the rest of the system governed by the relaxation rate  $\gamma_r$ .

### B. Dynamics from the modulation of other exchange couplings

So far, we focused on the effect of a modulated coupling strength  $J_3(t)$ . In general, a coupling of the optical phonon to the exchange couplings  $J_1$  or  $J_2$  is also possible [23]. The question arises whether the modulation of these couplings is qualitatively different compared to the modulation of  $J_3$  studied so far.

For this purpose, only slight modifications of the theory are necessary. The differential equations (24) are unchanged, but the prefactors  $\alpha_{\vec{k}}$  and  $\beta_{\vec{k}}$  have to be modified according to

$$\alpha_{\vec{k}} = \frac{A_{\vec{k}}}{\omega_{\vec{k}}} \left( 2 - 2 \frac{B_{\vec{k}}}{A_{\vec{k}}} \cos(k_c) \right) \quad (39a)$$

$$\beta_{\vec{k}} = \frac{A_{\vec{k}}}{\omega_{\vec{k}}} \left( -2 \frac{B_{\vec{k}}}{A_{\vec{k}}} + 2 \cos(k_c) \right) \quad (39b)$$

for discussing a driving via  $\delta J_1(t)$  and to

$$\alpha_{\vec{k}} = \frac{A_{\vec{k}}}{\omega_{\vec{k}}} \left( 6 - 2 \frac{B_{\vec{k}}}{A_{\vec{k}}} \gamma_{\Delta}(\vec{k}) \right) \quad (40a)$$

$$\beta_{\vec{k}} = \frac{A_{\vec{k}}}{\omega_{\vec{k}}} \left( -6 \frac{B_{\vec{k}}}{A_{\vec{k}}} + 2 \gamma_{\Delta}(\vec{k}) \right). \quad (40b)$$

when considering a driving via  $\delta J_2(t)$ .

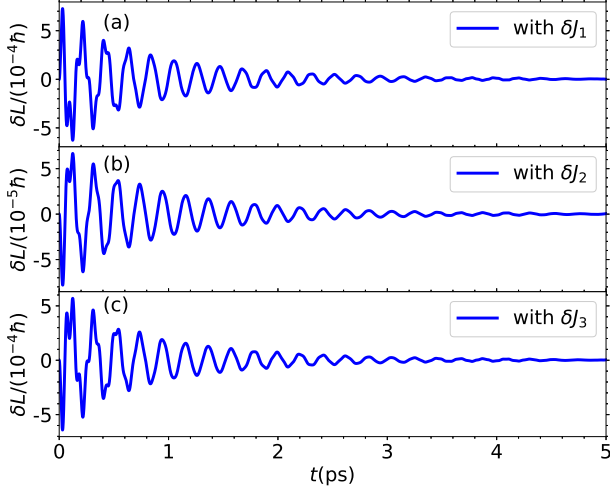


FIG. 14. Evolution of  $\delta L$  for modulated couplings (a)  $J_1$ , (b)  $J_2$ , and (c)  $J_3$  with relative amplitudes  $\kappa_i$ . Parameters:  $\kappa_i = 0.01$ ,  $M = 200$ ,  $\omega_0 = 30 \text{ ps}^{-1}$ ,  $\gamma = 1.0 \text{ ps}^{-1}$ ,  $\gamma_r = 0$ .

Figure 14 illustrates the change of the sublattice magnetization  $\delta L$  for all three cases; note the different scales of the  $y$  axes. In these calculations, we set  $\omega_0 = 30 \text{ ps}^{-1}$  and  $\gamma = 1 \text{ ps}^{-1}$  and neglect the magnon relaxation  $\gamma_r$ . The data of Fig. 14(c) is the same as in Fig. 5. All curves in Fig. 14 are very similar even though the coupling of the optical phonon is mediated by different Heisenberg terms. This is a consequence of the identical analytic structure of the differential equations governing the dynamics of the system.

However, the amplitude of  $\delta L$  is determined by the maximum relative deviation  $\max|\delta J_i|$  and the product  $B_{\vec{k}}\beta_{\vec{k}}$  since  $v_{\vec{k}}$  is proportional to  $\beta_{\vec{k}}$  (Eq. (27)) and is multiplied with  $B_{\vec{k}}$  to calculate  $\delta L$  (Eq. (17)). Because  $\beta_{\vec{k}}$  contain the number of nearest neighbors, a smaller value of  $J_i$  can be compensated by a large number of nearest neighbors. Therefore, with the parameter set used in this work, the strength of driving is approximately the same for  $J_1$  and  $J_3$  using the same relative coupling amplitude  $\kappa_1 = \kappa_3 = 0.01$ . In contrast, the effect of a modulated coupling  $J_2$  is significantly smaller.

In addition, the change of the sublattice magnetization induced by  $\delta J_1$  has the opposite sign compared to the change caused by  $\delta J_2$  or  $\delta J_3$ . This effect is traced back to the sign of the product  $\beta_{\vec{k}}B_{\vec{k}}$  in Eq. (34b) which is positive for  $J_1$  and negative for  $J_2$  and  $J_3$ .

In summary, the change of the sublattice magnetization predicted by the advocated model is up to a sign very

similar for the modulations of all couplings  $J_i$ . Hence, the analysis of the influence of the various parameters in the driving via  $\delta J_3(t)$  as presented in previous sections is sufficient to establish the essential physical response of  $\delta L$ .

## V. CONCLUSIONS

The research areas of magnonics and spintronics are currently attracting major interest [40, 41]. The idea to use magnetic excitations for information transport and processing is indeed very attractive because no physical object needs to be transported through the device. Hence such devices are considered strong candidates for reducing the energy consumption due to coherent information processing [42, 43].

One key issue for embedding such magnonics devices into the established semiconductor electronics is the conversion of spin signals into charge signals and vice versa at the highest possible operational speed. These considerations fuel the presently growing research fields of ultrafast magnonics and spintronics which aim at coupling spins and charges on the femtosecond time scales minimizing as much as possible the energy dissipation. A recent trend from the experimental side involves the optical activation of coherent phonons either via Raman scattering processes [32] or via resonant pumping [13, 21]. In this framework, it is a natural choice to investigate hexagonal MnTe since in this material the optical bandgap, i.e., the charge degree of freedom, is naturally coupled to both the spins [18, 19, 44] and to the lattice [20] in equilibrium.

Hence, in this article we pursued the idea that light triggers coherent lattice motion which in turn induces coherent oscillations of the sublattice magnetization. Aiming at  $\alpha$ -MnTe, we employed a Heisenberg model whose coupling constants are determined by data from inelastic neutron scattering [30]. The optically induced atomic displacements modulate the exchange couplings and thereby create pairs of magnons of opposite momenta in the considered isotropic spin model. We studied the dependence of the temporal evolution of the sublattice magnetization on the variation of parameters such as the amplitude of the modulation of the exchange coupling, the duration of the coherent lattice oscillation, its carrier frequency, and a phenomenological relaxation rate of the magnons. The used parameters are chosen in the experimentally relevant range [23].

In particular, we calculated the dynamics of the sublattice magnetization  $L(t)$  induced by the oscillating Heisenberg coupling  $J_3$  between third-nearest neighbors. The time-dependent deviation  $\delta L(t)$  to the equilibrium value is given by a weighted sum of the dynamics of all  $\vec{k}$ -modes. Since the differential equations describing the dynamics of the  $\vec{k}$ -modes remain diagonal in momentum space in linear spin wave theory and for the assumed relaxation mechanism, it is possible to gain analytic insight by analyzing individual  $\vec{k}$ -modes. We solved the differen-

tial equations in the presence of a driving term with some simplifying assumptions analytically as well as fully numerically. In this way, we have explained the properties of  $\delta L(t)$  and its dependence on the external parameters.

We found that the qualitative features depend only quantitatively on which exchange coupling is modulated by the optical excited coherent lattice mode. The exception to this rule is a sign change of the oscillations of  $\delta L(t)$  if the coupling  $J_1$  is modulated instead of  $J_2$  or  $J_3$ .

But except for this phase shift of  $\pi$  our observation has two implications: (i) generally, it demonstrates the generic nature of our approach, which is applicable to a wide class of materials and (ii) in the context of  $\alpha$ -MnTe, the calculated the modulation of the sublattice magnetization does not require the precise microscopic details of how the optically excited displacement mode influences the exchange paths, which is presently not known.

We stress that the computed effects in the sublattice magnetization  $L(t)$  are measurable experimentally as both the longitudinal and transversal femtosecond dynamics of  $L(t)$  can be detected by means of magneto-optical effects in a wide variety of materials [11, 45]. It is thus important to point out that the presented calculations for  $\alpha$ -MnTe can easily be adapted to any other ordered quantum antiferromagnetic system.

Furthermore, future research can extend the studied model in various directions: (i) The relaxation mechanism of magnons as considered here does not conserve the total spin [29]. More elaborate Lindblad operators can ensure the conservation of spin which holds for the dominant processes in many systems. (ii) We assume the unperturbed state, prior to the photoexcitation, to be in equilibrium at zero temperature. It is straightforward to include finite temperature. (iii) In linear spin wave theory we neglected the scattering of the magnons among themselves. Such interaction effects can be included on the level of Boltzmann equations, see for instance Ref. [46]. (iv) Finally, it is conceptually interesting to study the short coherent drive in the vicinity of thermal and quantum phase transitions in order to determine whether it is possible to drive the system from one phase into the other.

The ultrafast coherent control of macroscopic magnetic states is thus an exciting research field still in its infancy, from both the experimental and the theoretical side as well.

## VI. ACKNOWLEDGEMENTS

We acknowledge useful discussions with Mohsen Hafez-Torbati and Bruce Normand. This study was carried out in the International Collaborative Research Centre 160 (Project B8) funded by the Deutsche Forschungsgemeinschaft (DFG) and the Russian Foundation for Basic Research. Further support (GSU) by the DFG was obtained through the projects UH 90/13-1 and UH 90/14-1. D.B. acknowledges supports from the Deutsche Forschungsgemeinschaft (DFG) program BO5074/1-1.

### Appendix A: Analytical approximated solution of the differential equations

To calculate the dynamics analytically, we combine the terms  $v_{\vec{k}}(t)$  and  $w_{\vec{k}}(t)$  in the complex number  $z_{\vec{k}}(t) = v_{\vec{k}}(t) + iw_{\vec{k}}(t)$  obeying the differential equation

$$\frac{dz_{\vec{k}}}{dt} = 2i(\omega_{\vec{k}} + a(t)\alpha_{\vec{k}})z_{\vec{k}} - \gamma_r z_{\vec{k}} + if_{\vec{k}}(t) \quad (\text{A1})$$

with

$$f_{\vec{k}}(t) = 2a(t)\beta_{\vec{k}}(u_{\vec{k}}(t) + 1/2) \quad (\text{A2a})$$

$$a(t) = a_0 \cos(\omega_0 t) \exp(-\gamma t). \quad (\text{A2b})$$

This results from Eqs. (21), (24b), and (24c). Neglecting  $a(t)\alpha_{\vec{k}}$  relative to  $\omega_{\vec{k}} \gg a(t)\alpha_{\vec{k}}$  simplifies Eq.(A1) to

$$\frac{dz_{\vec{k}}}{dt} = (2i\omega_{\vec{k}} - \gamma_r)z_{\vec{k}} + if_{\vec{k}}(t). \quad (\text{A3})$$

For the estimated parameters relevant for experiment the approximation is well justified as we verified by comparing approximate analytical with numerical results without this approximation. The solution of Eq. (A3) is given by

$$z_{\vec{k}}(t) = i e^{(2i\omega_{\vec{k}} - \gamma_r)t} \int_0^t a(t')\beta_{\vec{k}}(2u_{\vec{k}}(t') + 1) e^{-(2i\omega_{\vec{k}} - \gamma_r)t'} dt'. \quad (\text{A4})$$

If we assume additionally that  $2u_{\vec{k}}(t') \ll 1$ , we can neglect  $u_{\vec{k}}(t')$ . This holds certainly for not too strong and not too long lasting driving. Then the integral in Eq. (A4) can be solved analytically

$$z_{\vec{k}}(t) = ia_0\beta_{\vec{k}} \left[ \frac{e^{-\gamma t}(\omega_0 \sin(\omega_0 t) - (2i\omega_{\vec{k}} + \gamma - \gamma_r) \cos(\omega_0 t))}{\omega_0^2 - (2\omega_{\vec{k}} - i(\gamma - \gamma_r))^2} + \frac{(2i\omega_{\vec{k}} + \gamma - \gamma_r)e^{2i\omega_{\vec{k}}t}e^{-\gamma t}}{\omega_0^2 - (2\omega_{\vec{k}} - i(\gamma - \gamma_r))^2} \right]. \quad (\text{A5})$$

### Appendix B: Evolution of the slowly varying part of the magnon occupation $u_{\vec{k}}$ .

Here we address the computation of the slow evolution of the magnon occupation upon driving by quickly oscillating terms. The starting point is the set of three

differential equations at each momentum  $\vec{k}$  in the Brill-

loun zone

$$\frac{du_{\vec{k}}^-}{dt} = 2a(t)\beta_{\vec{k}}^-w_{\vec{k}}^- \quad (\text{B1a})$$

$$\frac{dv_{\vec{k}}^-}{dt} = -2(\omega_{\vec{k}}^- + a(t)\alpha_{\vec{k}}^-)w_{\vec{k}}^- \quad (\text{B1b})$$

$$\frac{dw_{\vec{k}}^-}{dt} = 2(\omega_{\vec{k}}^- + a(t)\alpha_{\vec{k}}^-)v_{\vec{k}}^- + f_{\vec{k}}^-(t) \quad (\text{B1c})$$

$$\text{with } f_{\vec{k}}^-(t) := 2a(t)\beta_{\vec{k}}^-(u_{\vec{k}}^- + 1/2) \quad (\text{B1d})$$

where we omitted the phenomenological magnetic relaxation  $\gamma_r$ . Obviously, the momentum dependence enters only via the dispersion  $\omega_{\vec{k}}^-$ . We adapt the calculation for three-fold degenerate triplons in Ref. [29] to a system of magnons. First, we deal with a constant amplitude, i.e., the pulse lasts indefinitely. Second, we generalize the result to exponentially decaying driving term  $a(t)$ .

### 1. Driving by an indefinite oscillating term $a(t)$

We set  $a(t) = a_0 \cos(\omega_0 t)$ , define  $z_{\vec{k}}^-(t) = v_{\vec{k}}^-(t) + iw_{\vec{k}}^-(t)$ , and combine Eqs. (B1b) and (B1c)

$$\frac{dz_{\vec{k}}^-}{dt} = 2i(\omega_{\vec{k}}^- + a_0 \cos(\omega_0 t)\alpha_{\vec{k}}^-)z_{\vec{k}}^- + if_{\vec{k}}^-(t). \quad (\text{B2})$$

The solution of this differential equation reads

$$z_{\vec{k}}^-(t) = ie^{ih_{\vec{k}}^-(t)} \int_0^t f_{\vec{k}}^-(t') e^{-ih_{\vec{k}}^-(t')} dt' \quad (\text{B3a})$$

$$\text{with } h_{\vec{k}}^-(t) := 2 \int_0^t (\omega_{\vec{k}}^- + a_0 \alpha_{\vec{k}}^- \cos(\omega_0 t')) dt' \quad (\text{B3b})$$

$$= 2\omega_{\vec{k}}^- t + 2 \frac{a_0 \alpha_{\vec{k}}^-}{\omega_0} \sin(\omega_0 t) \quad (\text{B3c})$$

Expressing  $w_{\vec{k}}^-$  by the imaginary part of  $z_{\vec{k}}^-$  we find the solution for  $u_{\vec{k}}^-(t)$  by integrating Eq. (B1c)

$$u_{\vec{k}}^-(t) = 2a_0 \beta_{\vec{k}}^- \int_0^t \cos(\omega_0 t') \Im z_{\vec{k}}^- dt'. \quad (\text{B4})$$

In order to focus on the essential slow evolution of  $u_{\vec{k}}^-$  we average out the fast oscillation in  $u_{\vec{k}}^-(t)$  with frequency  $2\omega_0$  and higher. To this end, we replace  $\cos(\omega_0 t) e^{-ih_{\vec{k}}^-(t)}$  in Eq. (B3a) by its average over one period  $T_0 = 2\pi/\omega_0$ .

First, we consider the **resonant case**  $\omega_0 = 2\omega_{\vec{k}}$ . Then the relation

$$\phi^{-1} J_1(\phi) = \frac{1}{T_0} \int_0^{T_0} \cos(\omega_0 t') e^{-i\omega_0 t' - i\phi \sin(\omega_0 t')} dt' \quad (\text{B5})$$

with  $\phi = 2a_0 \alpha_{\vec{k}}^- / \omega_0$  is directly applicable. The replacement (B5) is well justified if the oscillations at  $\omega_0$  are much faster than the slow evolution. This is fulfilled if oscillation frequency in the THZ range or smaller are applied.

We obtain

$$z_{\vec{k}}^-(t) = i \frac{\beta_{\vec{k}}^- \omega_0}{\alpha_{\vec{k}}^-} J_1(\phi) e^{i_{\vec{k}} h_{\vec{k}}^-(t)} \int_0^t (u_{\vec{k}}^-(t') + 1/2) dt' \quad (\text{B6})$$

with the Bessel function of the first kind  $J_1(x)$ . Inserting this result into Eq. (B4) and using the averaging of Eq. (B5) in its complex conjugated form again yields

$$u_{\vec{k}}^-(t) = \Gamma^2 \Re \int_0^t \int_0^{t'} (u_{\vec{k}}^-(t'') + 1/2) dt'' dt' \quad (\text{B7a})$$

$$\Gamma := \left( \frac{\beta_{\vec{k}}^- \omega_0}{\alpha_{\vec{k}}^-} \right) J_1(\phi). \quad (\text{B7b})$$

Differentiating twice with respect to time leads to the simple differential equation

$$u_{\vec{k}}^{''}(t) = \Gamma^2 (u_{\vec{k}}^-(t) + 1/2). \quad (\text{B8})$$

For the relevant initial conditions  $u_{\vec{k}}^-(t=0) = 0$  and  $u_{\vec{k}}^{'}(t=0) = 0$  this is solved in a standard way yielding the result (29) in the main text as can be easily checked.

Second, we consider the off-resonant case with some detuning  $\delta := 2\omega_{\vec{k}}^- - \omega_0$ . We assume this detuning to be small so that the oscillations associated with it can be considered to be small  $|\delta| \ll \omega_0$ . Then we apply almost the same steps as before. Using the replacement (B5) for  $\omega_0$  we arrive at

$$z_{\vec{k}}^-(t) = i \frac{\beta_{\vec{k}}^- \omega_0}{\alpha_{\vec{k}}^-} J_1(\phi) e^{i_{\vec{k}} h_{\vec{k}}^-(t)} \int_0^t (u_{\vec{k}}^-(t') + 1/2) e^{-i\delta t'} dt'. \quad (\text{B9})$$

Then we insert this expression into (B6), use the averaging (B5) a second time, and obtain

$$u_{\vec{k}}^-(t) = \Gamma^2 \Re \int_0^t e^{i\delta t'} \int_0^{t'} e^{-i\delta t''} (u_{\vec{k}}^-(t'') + 1/2) dt'' dt'. \quad (\text{B10})$$

Due to the factors  $e^{i\delta t}$  and the real part taken on the right hand side this is not converted to a closed differential equation by double differentiation. But differentiating three times yields

$$u_{\vec{k}}^{'''}(t) = (\Gamma^2 - \delta^2) u_{\vec{k}}^{'}(t). \quad (\text{B11})$$

The initial conditions are  $u_{\vec{k}}^-(t=0) = 0$ ,  $u_{\vec{k}}^{'}(t=0) = 0$ , and  $u_{\vec{k}}^{''}(t=0) = \Gamma^2/2$ . The solution depends on the sign of  $\Gamma^2 - \delta^2$  and is given in the main text in (30).

For constant driving ( $\gamma = 0$ ), Fig. 15(a) displays the magnon occupation  $u_{\vec{k}}^-(t)$  for resonant (blue curve) and off-resonant driving of type (B) (red curve) as they are obtained by integrating the Eqs. (24) for  $\omega_{\vec{k}}^- = 50 \text{ ps}^{-1}$ . The numerical solution contains fast oscillations at frequency  $2\omega_0$  with very small amplitudes. But the slow evolution of  $u_{\vec{k}}^-(t)$  is well captured by Eqs. (29) and (30). To illustrate this point, we plot a zoom of the data of Fig. 15(a) in Fig. 15(b): the numerical solution wiggles fast around the analytic result as expected from the above derivation.

For small detuning,  $\Gamma > |\delta|$  (not shown), we obtain a monotonically increasing magnon occupation, very similar to the completely resonant case. This is important for the possibility to approximate the integral over the Brillouin zone by a finite sum over a discrete mesh of eigenfrequencies because the discretization generically prevents



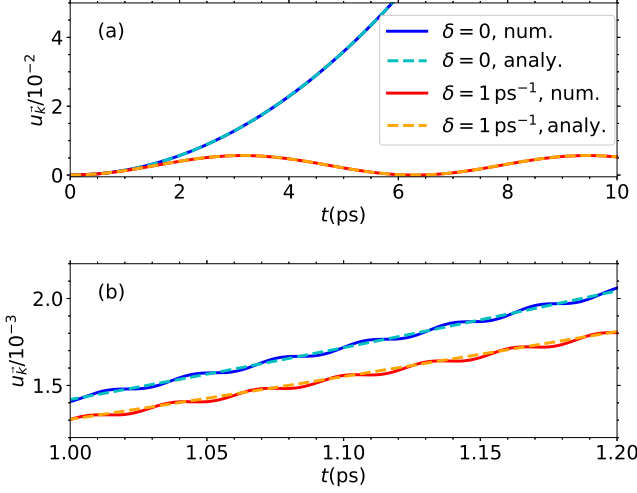


FIG. 15. The magnon occupation  $u_{\vec{k}}(t)$  of a specific magnon mode  $\omega_{\vec{k}} = 50 \text{ ps}^{-1}$  for resonant (dark and light blue) and off-resonant (red and orange) driving  $\delta = 1 \text{ ps}^{-1}$  with constant amplitude. The solid curves represent the full numerical solution while the dashed curves represent the analytical approximations Eqs. (29a) and (30c) with  $\kappa = 0.01, \Gamma = 0.0753 \text{ ps}^{-1}, \Gamma' = 0.9972 \text{ ps}^{-1}$ . Panel (a): full time interval; panel (b): zoom of panel (a) to show the fast oscillations.

perfect resonance. For larger detuning ( $\Gamma < |\delta|$ ), the magnon occupation displays the slow oscillations with the renormalized detuning  $\Gamma' < \delta$  as given by Eq. (30c).

## 2. Driving by a damped term $a(t)$

Here we consider the driving term

$$a(t) = a_0 \cos(\omega_0 t) \exp(-\gamma t), \quad (\text{B12})$$

Still, (B3a) holds if we adapt the definition of  $h_{\vec{k}}$  according to

$$h_{\vec{k}}(t) := 2 \int_0^t (\omega_{\vec{k}} + a_0 \alpha_{\vec{k}} \cos(\omega_0 t') \exp(-\gamma t')) dt' \quad (\text{B13a})$$

$$\begin{aligned} &= 2\omega_{\vec{k}} t \\ &+ 2 \frac{a_0 \alpha_{\vec{k}}}{\omega_0^2 + \gamma^2} [e^{-\gamma t} (\omega_0 \sin(\omega_0 t) - \gamma \cos(\omega_0 t)) + \gamma] \end{aligned} \quad (\text{B13b})$$

$$\approx 2\omega_{\vec{k}} t. \quad (\text{B13c})$$

Unfortunately, the modified averaging similar to (B5) can only be performed in the limit of weak driving  $a_0 \rightarrow 0$  where  $\Gamma = a_0 \beta_{\vec{k}}$ . Otherwise, a time dependence remains in  $\phi \propto \exp(-\gamma t)$ . But most calculations are indeed done for weak driving and to understand the effects of these pulses qualitatively the limit of weak driving is relevant. So we actually use the approximation Eq. (B13c) and the

averaging

$$1/2 = \frac{1}{T_0} \int_0^{T_0} \cos(\omega_0 t') e^{-i\omega_0 t'} dt' \quad (\text{B14})$$

to arrive from (B3a) at

$$z_{\vec{k}}(t) = i\Gamma e^{i\vec{k} \cdot h_{\vec{k}}(t)} \int_0^t e^{-\gamma t'} (u_{\vec{k}}(t') + 1/2) dt'. \quad (\text{B15})$$

We insert this result in

$$u_{\vec{k}}(t) = 2\Gamma \int_0^t \cos(\omega_0 t') e^{-\gamma t} \Im z_{\vec{k}} dt', \quad (\text{B16})$$

apply the averaging a second time, and finally obtain

$$u_{\vec{k}}(t) = \Gamma^2 \int_0^t dt' e^{-\gamma t'} \int_0^{t'} dt'' e^{-\gamma t''} (u_{\vec{k}}(t'') + 1/2). \quad (\text{B17})$$

At this stage, one can proceed in two ways. One is to focus on low occupations  $2u_{\vec{k}} \ll 1$  so that  $u_{\vec{k}}$  in the integrand can be neglected. Double integration straightforwardly yields Eq. (31) given in the main text. Alternatively, twice differentiating of Eq. (B17) yields the differential equation

$$u_{\vec{k}}'' = \Gamma^2 e^{-2\gamma t} (u_{\vec{k}} + 1/2) - \gamma u_{\vec{k}}' \quad (\text{B18})$$

which needs to be solved for the initial conditions  $u_{\vec{k}}(0) = 0 = u_{\vec{k}}'(0)$ . No closed expression can be found for its solution, but it is easily integrated by any computer algebra program.

Similarly, we can tackle the detuned case yielding

$$u_{\vec{k}}(t) = \Gamma^2 \Re \int_0^t dt' e^{(i\delta - \gamma)t'} \int_0^{t'} dt'' e^{-(i\delta + \gamma)t''} \left( u_{\vec{k}}(t'') + \frac{1}{2} \right). \quad (\text{B19})$$

Again, one can proceed in two ways. One is to focus on low occupations  $2u_{\vec{k}} \ll 1$  so that  $u_{\vec{k}}$  in the integrand can be neglected. Double integration straightforwardly yields Eq. (32) given in the main text. Alternatively, a differentiation of Eq. (B19), multiplication with  $\exp(\gamma t)$  and two more differentiation yield the differential equation

$$\begin{aligned} u_{\vec{k}}''' &= (\Gamma^2 e^{-2\gamma t} - \delta^2 - \gamma^2) u_{\vec{k}}' \\ &- 2\gamma u_{\vec{k}}'' - \gamma \Gamma^2 e^{-2\gamma t} (u_{\vec{k}}(t) + 1/2). \end{aligned} \quad (\text{B20})$$

This equation can easily be solved numerically with the initial conditions  $u_{\vec{k}}(0) = 0 = u_{\vec{k}}'(0)$  and  $u_{\vec{k}}''(0) = \Gamma^2/2$ .

## 3. Driving by a damped term $a(t)$ in presence of magnon relaxation

Here we extend the previous arguments to the case where the phenomenological relaxation of magnetic modes is included. That means that  $\gamma_r > 0$  is considered and we start from the general Eqs. (24) and (A1). Integrating  $u_{\vec{k}}$  yields

$$u_{\vec{k}}(t) = 2\Gamma e^{-\gamma_r t} \int_0^t \cos(\omega_0 t') e^{(\gamma_r - \gamma)t'} \Im z_{\vec{k}}(t') dt'. \quad (\text{B21})$$

The integration of (A1) yields

$$z_k^-(t) = ie^{ih_k - \gamma_r t} \int_0^t f_k^-(t') e^{-ih_k + \gamma_r t'} dt'. \quad (\text{B22})$$

As before we average the quickly oscillating part in (B22) using (B14) and insert the result into (B21). Then we average a second time using (B14) to obtain

$$u_k^-(t) = \Gamma^2 e^{-\gamma_r t} \int_0^t dt' e^{-\gamma t'} \int_0^{t'} dt'' e^{-\gamma t''} (u_k^- + e^{\gamma_r t''} / 2) \quad (\text{B23})$$

in the resonant case, i.e., for  $\omega_0 = 2\omega_k^-$ . For deriving the corresponding differential equation it is convenient to define

$$\tilde{u}_k^-(t) := \exp(\gamma_r t) u_k^-(t). \quad (\text{B24})$$

Differentiating  $\tilde{u}_k^-(t)$  twice yields the differential equation

$$\tilde{u}_k^{\prime\prime}(t) = -\gamma \tilde{u}_k' + \Gamma^2 e^{-2\gamma t} (e^{-\gamma_r t} \tilde{u}_k^- + e^{\gamma_r t} / 2), \quad (\text{B25})$$

which is to be solved for  $\tilde{u}_k^-(0) = 0 = \tilde{u}_k^{\prime}(0)$ .

Alternatively, we restrict ourselves to small values of  $u_k^-$  and directly integrate (B23) providing us with

$$u_k^-(t) = \frac{\Gamma^2 (\gamma - \gamma_r) e^{-\gamma_r t} + \gamma e^{-2\gamma t} - (2\gamma - \gamma_r) e^{-(\gamma + \gamma_r) t}}{2 \gamma (\gamma - \gamma_r) (2\gamma - \gamma_r)}. \quad (\text{B26})$$

Note that this leads to an initial rise followed by a maximum and subsequent bi-exponential decay governed by  $e^{-\gamma_r t}$  and  $e^{-\gamma t}$ .

Finally, we address the detuned case for which go again through the same steps as above. Instead of Eq. (B23) we obtain

$$u_k^-(t) = \Gamma^2 e^{-\gamma_r t} \Re \int_0^t dt' e^{(i\delta - \gamma)t'} \int_0^{t'} dt'' e^{-(i\delta + \gamma)t''} (u_k^- + e^{\gamma_r t''} / 2). \quad (\text{B27})$$

Appropriate triple differentiation allows to derive the differential equation

$$\tilde{u}_k^{\prime\prime\prime}(t) = -2\gamma \tilde{u}_k^{\prime\prime} - (\delta^2 + \gamma^2 - \Gamma^2 e^{-(2\gamma + \gamma_r)t}) \tilde{u}_k' - (\gamma + \gamma_r) \Gamma^2 e^{-(2\gamma + \gamma_r)t} \tilde{u}_k^- - (\gamma - \gamma_r) \Gamma^2 e^{-(2\gamma + \gamma_r)t} / 2 \quad (\text{B28})$$

which needs to be solved for the initial conditions  $\tilde{u}_k^-(0) = 0 = \tilde{u}_k^{\prime}(0)$  and  $\tilde{u}_k^{\prime\prime}(0) = \Gamma^2 / 2$ .

For small values of  $u_k^-$  we can integrate (B27) to obtain

$$u_k^-(t) = \frac{\Gamma^2}{2} \left( \frac{(\gamma - \gamma_r) e^{-2\gamma t}}{(2\gamma - \gamma_r)(\delta^2 + (\gamma - \gamma_r)^2)} - \frac{[(\delta^2 - \gamma\gamma_r + \gamma^2) \cos(\delta t) + \delta\gamma_r \sin(\delta t)] e^{-(\gamma + \gamma_r)t}}{(\delta^2 + \gamma^2)(\delta^2 + (\gamma - \gamma_r)^2)} + \frac{\gamma e^{-\gamma_r t}}{(2\gamma - \gamma_r)(\delta^2 + \gamma^2)} \right). \quad (\text{B29})$$

- 
- [1] A. Kirilyuk, A. V. Kimel, and T. Rasing, Ultrafast optical manipulation of magnetic order, *Rev. Mod. Phys.* **82**, 2731 (2010).
- [2] A. Kimel, A. Kirilyuk, P. Usachev, R. Pisarev, A. Balbashov, and T. Rasing, Ultrafast non-thermal control of magnetization by instantaneous photomagnetic pulses, *Nature* **435**, 655 (2005).
- [3] E. Beaurepaire, J.-C. Merle, A. Daunois, and J.-Y. Bigot, Ultrafast spin dynamics in ferromagnetic nickel, *Phys. Rev. Lett.* **76**, 4250 (1996).
- [4] A. Stupakiewicz, K. Szerenos, D. Afanasiev, A. Kirilyuk, and A. Kimel, Ultrafast nonthermal photo-magnetic recording in a transparent medium, *Nature* **542**, 71 (2017).
- [5] B. Koopmans, G. Malinowski, F. Dalla Longa, D. Steiauf, M. Fähnle, T. Roth, M. Cinchetti, and M. Aeschlimann, Explaining the paradoxical diversity of ultrafast laser-induced demagnetization, *Nature materials* **9**, 259 (2010).
- [6] M. Hofherr, S. Häuser, J. K. Dewhurst, P. Tengdin, S. Sakshath, H. T. Nembach, S. T. Weber, J. M. Shaw, T. J. Silva, H. C. Kapteyn, M. Cinchetti, B. Rethfeld, M. M. Murnane, D. Steil, B. Stadtmüller, S. Sharma, M. Aeschlimann, and S. Mathias, Ultrafast optically induced spin transfer in ferromagnetic alloys, *Science Advances* **6** (2020).
- [7] D. Afanasiev, B. A. Ivanov, A. Kirilyuk, T. Rasing, R. V. Pisarev, and A. V. Kimel, Control of the ultrafast photoinduced magnetization across the morin transition in  $\text{DyFeO}_3$ , *Phys. Rev. Lett.* **116**, 097401 (2016).
- [8] S. L. Johnson, R. A. de Souza, U. Staub, P. Beaud,

- E. Möhr-Vorobeva, G. Ingold, A. Caviezel, V. Scagnoli, W. F. Schlotter, J. J. Turner, O. Krupin, W.-S. Lee, Y.-D. Chuang, L. Patthey, R. G. Moore, D. Lu, M. Yi, P. S. Kirchmann, M. Trigo, P. Denes, D. Doering, Z. Hussain, Z.-X. Shen, D. Prabhakaran, and A. T. Boothroyd, *Femtosecond Dynamics of the Collinear-to-Spiral Antiferromagnetic Phase Transition in CuO*, *Phys. Rev. Lett.* **108**, 037203 (2012).
- [9] D. Bossini, K. Konishi, S. Toyoda, T. Arima, J. Yumoto, and M. Kuwata-Gonokami, *Femtosecond activation of magnetoelectricity*, *Nat. Phys.* **14**, 370 (2018).
- [10] D. Bossini, S. Dal Conte, Y. Hashimoto, A. Secchi, R. Pisarev, T. Rasing, G. Cerullo, and A. Kimel, *Macrospin dynamics in antiferromagnets triggered by sub-20 femtosecond injection of nanomagnons*, *Nature communications* **7**, 1 (2016).
- [11] D. Bossini, A. M. Kalashnikova, R. V. Pisarev, T. Rasing, and A. V. Kimel, *Controlling coherent and incoherent spin dynamics by steering the photoinduced energy flow*, *Phys. Rev. B* **89**, 060405(R) (2014).
- [12] T. Satoh, R. Iida, T. Higuchi, M. Fiebig, and T. Shimura, *Writing and reading of an arbitrary optical polarization state in an antiferromagnet*, *Nature Photonics* **9**, 25 (2015).
- [13] T. F. Nova, A. Cartella, A. Cantaluppi, M. Först, D. Bossini, R. V. Mikhaylovskiy, A. V. Kimel, R. Merlin, and A. Cavalleri, *An effective magnetic field from optically driven phonons*, *Nature Physics* **13**, 132 (2017).
- [14] P. Němec, M. Fiebig, T. Kampfrath, and A. V. Kimel, *Antiferromagnetic opto-spintronics*, *Nature Physics* **14**, 229 (2018).
- [15] O. Gomonay and D. Bossini, *Linear and nonlinear spin dynamics in multidomain magnetoelastic antiferromagnets*, *Journal of Physics D: Applied Physics* **54**, 374004 (2021).
- [16] S. R. Mobasser and T. R. Hart, *Raman Scattering From Phonons And Magnons In Magnetic Semiconductor, MnTe*, in *Spectroscopic Characterization Techniques for Semiconductor Technology of Applied Crystallography* **44**, 1272 (2011). Vol. 0524, edited by F. H. Pollak and R. Tsu, International Society for Optics and Photonics (SPIE, 1985) pp. 137 – 144.
- [17] D. Kriegner, K. Výborný, K. Olejník, H. Reichlová, V. Novák, X. Marti, J. Gazquez, V. Saidl, P. Němec, V. V. Volobuev, G. Springholz, V. Holý, and T. Jungwirth, *Multiple-stable anisotropic magnetoresistance memory in antiferromagnetic MnTe*, *Nat Commun* **7**, 11623 (2016).
- [18] C. Ferrer-Roca, A. Segura, C. Reig, and V. Muñoz, *Temperature and pressure dependence of the optical absorption in hexagonal MnTe*, *Phys. Rev. B* **61**, 13679 (2000).
- [19] D. Bossini, M. Terschanski, F. Mertens, G. Springholz, A. Bonanni, G. S. Uhrig, and M. Cinchetti, *Exchange-mediated magnetic blue-shift of the band-gap energy in the antiferromagnetic semiconductor MnTe*, *New Journal of Physics* **22**, 083029 (2020).
- [20] J. Zhang, Q. Lian, Z. Pan, W. Bai, J. Yang, Y. Zhang, X. Tang, and J. Chu, *Spin-phonon coupling and two-magnons scattering behaviors in hexagonal NiAs-type antiferromagnetic MnTe epitaxial films*, *Journal of Raman Spectroscopy* **51**, 1383 (2020).
- [21] M. Först, C. Manzoni, S. Kaiser, Y. Tomioka, Y. Tokura, R. Merlin, and A. Cavalleri, *Nonlinear phononics as an ultrafast route to lattice control*, *Nature Physics* **7**, 854 (2011).
- [22] Y. Hashimoto, D. Bossini, T. H. Johansen, E. Saitoh, A. Kirilyuk, and T. Rasing, *Frequency and wavenumber selective excitation of spin waves through coherent energy transfer from elastic waves*, *Phys. Rev. B* **97**, 140404(R) (2018).
- [23] D. Bossini, S. D. Conte, M. Terschanski, G. Springholz, A. Bonanni, K. Deltenre, F. Anders, G. Uhrig, G. Cerullo, and M. Cinchetti, *Femtosecond phononic coupling to both spins and charges in a room temperature antiferromagnetic semiconductor*, arXiv:2110.15173 (2021).
- [24] S. Mu, R. P. Hermann, S. Gorsse, H. Zhao, M. E. Manley, R. S. Fishman, and L. Lindsay, *Phonons, magnons, and lattice thermal transport in antiferromagnetic semiconductor MnTe*, *Phys. Rev. Materials* **3**, 025403 (2019).
- [25] P. A. Fleury and R. Loudon, *Scattering of light by one- and two-magnon excitations*, *Phys. Rev.* **166**, 514 (1968).
- [26] B. S. Shastry and B. I. Shraiman, *Theory of Raman scattering in Mott-Hubbard systems*, *Phys. Rev. Lett.* **65**, 1068 (1990).
- [27] E. V. Boström, T. S. Parvini, J. W. McIver, A. Rubio, S. V. Kusminskiy, and M. A. Sentef, *All-optical generation of antiferromagnetic magnon currents via the magnon circular photogalvanic effect* (2021), *PhysRevB.104.L100404*.
- [28] M. Fechner, A. Sukhov, L. Chotorlishvili, C. Kenel, J. Berakdar, and N. A. Spaldin, *Magnetophononics: Ultrafast spin control through the lattice*, *Phys. Rev. Materials* **2**, 064401 (2018).
- [29] M. Yarmohammadi, C. Meyer, B. Fauseweh, B. Normand, and G. S. Uhrig, *Dynamical properties of a driven dissipative dimerized  $S = \frac{1}{2}$  chain*, *Phys. Rev. B* **103**, 045132 (2021).
- [30] W. Szuszkiewicz, E. Dynowska, B. Witkowska, and B. Hennion, *Spin-wave measurements on hexagonal MnTe of NiAs-type structure by inelastic neutron scattering*, *Phys. Rev. B* **73**, 104403 (2006).
- [31] K. Momma and F. Izumi, *VESTA3 for three-dimensional visualization of crystal, volumetric and morphology data*, *Journal of Applied Crystallography* **44**, 1272 (2011).
- [32] R. Merlin, *Generating coherent THz phonons with light pulses*, *Solid State Communications* **102**, 207 (1997), highlights in *Condensed Matter Physics and Materials Science*.
- [33] H. J. Zeiger, J. Vidal, T. K. Cheng, E. P. Ippen, G. Dresselhaus, and M. S. Dresselhaus, *Theory for dispersive excitation of coherent phonons*, *Phys. Rev. B* **45**, 768 (1992).
- [34] M. Takahashi, *Modified spin-wave theory of a square-lattice antiferromagnet*, *Phys. Rev. B* **40**, 2494 (1989).
- [35] C. J. Hamer, Z. Weihong, and P. Arndt, *Third-order spin-wave theory for the Heisenberg antiferromagnet*, *Phys. Rev. B* **46**, 6276 (1992).
- [36] T. Holstein and H. Primakoff, *Field dependence of the intrinsic domain magnetization of a ferromagnet*, *Phys. Rev.* **58**, 1098 (1940).
- [37] T. Hanisch, B. Kleine, A. Ritzl, and E. Müller-Hartmann, *Ferromagnetism in the Hubbard model: instability of the Nagaoka state on the triangular, honeycomb and kagome lattices*, *Annalen der Physik* **507**, 303 (1995).
- [38] H.-P. Breuer and F. Petruccione, *The Theory of Open Quantum Systems* (Clarendon Press, Oxford, 2006).
- [39] W. H. Press, S. A. Teukolsky, W. T. Vetterling, and B. P. Flannery, *Numerical Recipes 3rd Edition: The Art of Scientific Computing*, 3rd ed. (Cambridge University Press,

- USA, 2007).
- [40] A. Barman, G. Gubbiotti, S. Ladak, A. O. Adeyeye, M. Krawczyk, J. Gräfe, C. Adelman, S. Cotozana, A. Naeemi, V. I. Vasyuchka, B. Hillebrands, S. A. Nikitov, H. Yu, D. Grundler, A. V. Sadovnikov, A. A. Grachev, S. E. Sheshukova, J.-Y. Duquesne, M. Marangolo, G. Csaba, W. Porod, V. E. Demidov, S. Urazhdin, S. O. Demokritov, E. Albisetti, D. Petti, R. Bertacco, H. Schultheiss, V. V. Kruglyak, V. D. Poimanov, S. Sahoo, J. Sinha, H. Yang, M. Münzenburg, T. Moriyama, S. Mizukami, P. Landeros, R. A. Gallardo, G. Carlotti, J.-V. Kim, R. L. Stamps, R. E. Camley, B. Rana, Y. Otani, W. Yu, T. Yu, G. E. W. Bauer, C. Back, G. S. Uhrig, O. V. Dobrovolskiy, B. Budinska, H. Qin, S. van Dijken, A. V. Chumak, A. Khitun, D. E. Nikonov, I. A. Young, B. W. Zingsem, and M. Winklhofer, The 2021 Magnonics Roadmap, *Journal of Physics: Condensed Matter* **33**, 413001 (2021).
- [41] Malki, M. and Uhrig, G. S., Topological magnetic excitations, *EPL* **132**, 20003 (2020).
- [42] M. Jäckl, V. I. Belotelov, I. A. Akimov, I. V. Savochkin, D. R. Yakovlev, A. K. Zvezdin, and M. Bayer, Magnon accumulation by clocked laser excitation as source of long-range spin waves in transparent magnetic films, *Phys. Rev. X* **7**, 021009 (2017).
- [43] I. Bertelli, J. J. Carmiggelt, T. Yu, B. G. Simon, C. C. Pothoven, G. E. W. Bauer, Y. M. Blanter, J. Aarts, and T. van der Sar, Magnetic resonance imaging of spin-wave transport and interference in a magnetic insulator, *Science Advances* **6**, eabd3556 (2020).
- [44] M. Hafez-Torbati, D. Bossini, F. B. Anders, and G. S. Uhrig, Magnetic Blue-Shift of Mott Gaps (2020), arXiv:2012.04018 [cond-mat.str-el].
- [45] D. Bossini and T. Rasing, Femtosecond optomagnetism in dielectric antiferromagnets, *Phys. Scr.* **92**, 024002 (2017).
- [46] M. H. Kalthoff, D. M. Kennes, A. J. Millis, and M. A. Sentef, Nonequilibrium phase transition in a driven-dissipative quantum antiferromagnet, arXiv **2107.03841** (2021).